J. Fluid Mech. (1995), *vol.* 293, *pp.* 147–180

Numerical simulations of the effect of hydrodynamic interactions on diffusivities of integral membrane proteins

By TRAVIS L. DODD[1], DANIEL A. HAMMER[1], ASHOK S. SANGANI[2] AND DONALD L. KOCH[1]

[1] School of Chemical Engineering, Cornell University, Ithaca, NY 14853, USA

[2] Department of Chemical Engineering and Materials Science, Syracuse University, Syracuse, NY 13244, USA

(Received 17 June 1994 and in revised form 20 January 1995)

Proteins in a biological membrane can be idealized as disks suspended in a thin viscous sheet surrounded by a fluid of lower viscosity (Saffman 1976). To determine the effect of hydrodynamic interactions on protein diffusivities in non-dilute suspensions, we numerically solve the Stokes equations of motion for a system of disks in a bounded periodic two-dimensional fluid using a multipole expansion technique. We consider both free suspensions, in which all the proteins are mobile, and fixed beds, in which a fraction of the proteins are fixed. For free suspensions, we determine both translational and rotational short-time self-diffusivities and the gradient diffusivity as a function of the area fraction of the disks. The translational self- and gradient diffusivities computed in this way grow logarithmically with the number of disks owing to Stokes paradox; to obtain finite values, we renormalize our simulation results by treating long-range interactions in terms of a membrane with an enhanced viscosity in contact with a low-viscosity three-dimensional fluid. The diffusivities in fixed beds require no such adjustment because, at non-dilute area fractions of disks, the Brinkman screening of hydrodynamic interactions is more important that the viscous drag due to the surrounding three-dimensional fluid in limiting the range of hydrodynamic interactions. The diffusivities are determined as functions of the area fractions of both mobile and fixed proteins. We compare our results for diffusivities with experimental measurements of long-time protein self-diffusivity after adjusting our short-time diffusivities calculations in an approximate way to account for effects of hindered diffusion due to volume exclusion, and find very good agreement between the two.

1. Introduction

The diffusion of integral membrane proteins (or receptors) within the membrane plays an important role in physiological responses of the cell. For example, the diffusion-limited reaction of two integral membrane proteins (F_c receptors) in the membrane of an immunological cell called a basophil is responsible for the release of histamine into the blood stream in an acute allergic response (Metzger & Kinet 1988). The basis of much of the present understanding of the role of fluid mechanics in diffusion of integral membrane proteins is a model for the diffusion of a single protein presented by Saffman & Delbrück (1975) and Saffman (1976) which is described later in this introduction.

It has been observed that the diffusion of proteins is a strong function of their concentration (Scalletar & Abney 1991). In addition, the diffusion rate is much lower

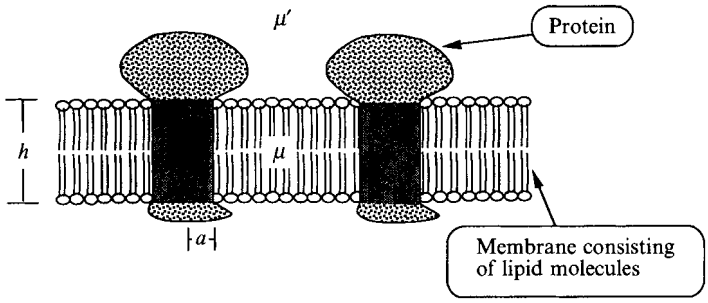

FIGURE 1. Sketch of a typical membrane cross-section containing proteins (taken from Bussell *et al.* 1992). The proteins have large hydrophillic head groups outside the bilayer and a hydrophobic cylindrical section suspended in a lipid bilayer.

in plasma membranes, in which some of the proteins are held fixed by attachment to the cytoskeleton, than it is in reconstituted membranes, which lack such constraints. Previous studies (Scalletar & Abney 1991) which have considered thermodynamic interactions of proteins in terms of volume exclusion effects and inter-particle potential forces but neglected their hydrodynamic interactions failed to adequately explain these experimental trends.

Recently, Bussell, Koch & Hammer (1992) extended Saffman's analysis by considering the relative diffusion of two proteins in a membrane. By combining their results for relative diffusion with the ensemble averaging techniques developed in the study of suspensions of Brownian spheres (Batchelor 1976, 1982; Hinch 1977), Bussell, Koch & Hammer (1994) determined the first effects of hydrodynamic interactions on the short- and long-time self-diffusivities and the collective mobility in a membrane with a low protein area fraction ϕ. In subsequent studies (Bussell, Koch & Hammer 1995*a*, *b*), these investigators combined their hydrodynamic analysis with results obtained from simulations of Saxton (1987, 1990), which account for the thermodynamic effects such as volume exclusion but not the hydrodynamic interactions among proteins, and the resulting long-time self-diffusivities were compared with those measured experimentally in several non-dilute protein–membrane systems. From these studies, it is clear that hydrodynamic interactions significantly affect the diffusivities and that the combination of hydrodynamic and thermodynamic (or non-hydrodynamic Brownian/Monte Carlo simulations) interactions can at least approximately account for both the large decrease in diffusivity with increasing ϕ and the much smaller rates of diffusion in plasma as compared to reconstituted membranes with the same ϕ.

The purpose of the present contribution is to provide more accurate results for the mobilities (or short-time diffusivities) in non-dilute membranes. This is accomplished through the use of numerical simulations based on multipole expansion techniques similar to those commonly in use for suspensions of spherical particles (Phillips, Brady & Bossis 1988; Ladd 1988, 1989, 1990; Mo & Sangani 1994; Sangani & Mo 1994).

Our work, like that of Bussell *et al.* (1992, 1994, 1995*a*, *b*), is based on the model proposed by Saffman (1976). A sketch of integral membrane proteins (IMPs) in a bilipid cell membrane is shown in figure 1. The hydrophobic and hydrophillic parts of IMPs, indicated respectively by the dotted and shaded regions, restrict the IMPs motion to the plane of the membrane. The size of a typical IMP is much greater than the lipid molecules and therefore the lipid phase is treated as an incompressible Newtonian continuum with viscosity μ. The surrounding aqueous phase on either side of the membrane is treated as a Newtonian continuum with viscosity μ'. The

proteins are idealized to be cylindrical and monodispersed with radius a and height h. The short-time self-diffusivity is then given by the well-known expression first derived by Einstein (1906)

$$\boldsymbol{D}_s = \boldsymbol{m}_s k_B T, \tag{1}$$

where k_B is the Boltzmann constant, T is the absolute temperature, and $\boldsymbol{m}_s$ is the self-mobility defined as the velocity with which a particle (protein) moves when acted upon by a force of unit magnitude, the force on all the other (mobile) particles in the suspension being zero. The original derivation due to Einstein considered only dilute Brownian suspensions, but arguments leading to (1) were later extended by Batchelor (1976) who showed that the above result applies to non-dilute suspensions as well provided that the diffusivity and mobility are treated as instantaneous configuration-dependent tensors. Ermak & McCammon (1978) used an alternative formulation based on a Langevin equation to derive the same result for the short-time self-diffusivity. Here, by short time we mean time small compared with the time it takes for the spatial configuration of particles to change appreciably but large compared with the viscous relaxation time of particle motion.

Saffman (1976) considered the dilute limit in which the hydrodynamic interactions with the other proteins in the membrane can be neglected. Furthermore, since λ defined by

$$\lambda = \mu h/(\mu' a) \tag{2}$$

is typically of $O(10^2$–$10^3)$ owing to the high viscosity of the lipid phase compared with the aqueous phase, he determined the mobility of the cylindrical particle when $\lambda \gg 1$. In this limit, the viscous resistance of the aqueous phase is negligible on the lengthscale a of protein radius and the velocity disturbance caused by the protein motion is essentially two-dimensional. Since the Reynolds number of the flow is very small, this velocity disturbance, however, grows logarithmically with the distance r from the centre of the protein owing to the well-known Stokes paradox according to which there does not exist a decaying solution to the Stokes equations of motion for the flow induced by a point force in a two-dimensional space. Saffman pointed out that the two-dimensional Stokes flow approximation, however, is not uniformly valid in space and that the viscous resistance due to the aqueous phase will become important at the scale of length $a\lambda$. Thus, by using the method of matched asymptotic expansions, in which the flow is approximated to be two-dimensional in the inner region of scale a and three-dimensional in the outer region of scale $a\lambda$, he showed that the diffusivity is given by

$$D_0(\lambda) = m_0 k_B T = \frac{k_B T}{4\pi\mu h}[\log\lambda - \gamma], \tag{3}$$

where $\gamma = 0.577216\ldots$ is the Euler's constant, and the subscript 0 is used to indicate that the result applies in the limit $\phi \to 0$. Since in this limit the difference between various different kinds of diffusivities vanishes, we have removed the subscript s from (1). Note also that the diffusivity is now a scalar quantity.

Saffman (1976) also considered the problem of determining the rotational diffusivity of proteins at small ϕ. Here, the mobility is defined as the angular velocity with which the particle rotates when acted upon by a torque of unit magnitude. This is a relatively straightforward calculation since the velocity induced by the point torque decays in a two-dimensional space, and, consequently, there is no need to account for the aqueous-phase viscous resistance. His result for the rotational diffusivity is

$$D_{r,0} = m_{r,0} k_B T = k_B T/(4\pi\mu h a^2). \tag{4}$$

Note that the rotational diffusivity defined here has units of inverse time. The rotational diffusion considered here is for rotation of the IMP on its axis; the rotation of the axis of the IMP is restricted by hydrophobic/hydrophilic interactions.

Saffman's analysis for translational diffusion is applicable to situations in which the aqueous-phase resistance is the most important mechanism responsible for the decay of velocity disturbance at great distances from the moving particle. This is true for most reconstituted and organelle membranes but not for plasma membranes as pointed out by Bussell *et al.* (1995*b*). In the latter case, some of the proteins at any given instant are held fixed by attachments to the fibrous cytoskeleton below the membrane. Thus, the appropriate model for plasma membranes must treat diffusion of mobile proteins through a fixed bed of immobilized proteins. This changes the hydrodynamics considerably. Now the velocity disturbance caused by the mobile protein decays like r^{-2} with the distance r in the outer region, i.e. $r \gg a\phi_i^{-1/2}$, due to the phenomenon known as Brinkman screening (Brinkman 1947; Howells 1974; Hinch 1977; Bussell *et al.* 1995*b*). Here, ϕ_i is the area fraction of immobile proteins. Of course, in the limit of vanishingly small ϕ (and hence ϕ_i) the result (3) is still valid. However, for most applications involving plasma membranes, the length $a\phi_i^{-1/2}$ based on Brinkman screening is much smaller than the length $a\lambda$ at which the effect of aqueous-phase viscous resistance becomes appreciable, and, consequently, we can set $\lambda = \infty$ for such suspensions. Thus, the hydrodynamics in plasma membranes are entirely two-dimensional.

As mentioned earlier, our study is focused on determining diffusivities in non-dilute membranes. Thus, for plasma membranes, we shall consider a suspension of mobile proteins diffusing in a fixed bed of immobilized proteins, whereas all of the proteins in the reconstituted and organelle membranes will be mobile. As explained above, two-dimensional simulations are adequate for determining diffusivities in plasma membranes. However, the application of purely two-dimensional simulation results to predict diffusivities in the reconstituted membranes requires a further step to account for the influence of the aqueous phase on a lengthscale $a\lambda$. We exploit the fact that the effect of proteins on the long-range velocity disturbances can be modelled simply as a change in the effective viscosity of the membrane to provide an analytical adjustment of our two-dimensional numerical solution to account for the behaviour of the three-dimensional membrane/aqueous fluid system.

Our simulation technique is similar to that described by Sangani & Mo (1994) for suspensions of spherical particles. This method is based on a multipole expansion for the velocity disturbance caused by each particle. However, when the particles become sufficiently close, the lubrication flow is treated by including analytically determined lubrication forces and torques acting on the particles. In addition, a contribution to the fluid velocity resulting from these lubrication forces is expressed in terms of velocity induced by force multipoles situated at the centre of the gap between the particles. The separate treatment of lubrication forces allows us to use a much smaller number of multipoles than would be required in simulations which simply rely upon the multipole expansion about the centre of each particle to resolve the lubrication flows. It should be noted that the two-dimensional flow considered here is particularly challenging for numerical simulations because both the long-range interactions and the short-range lubrication forces are stronger than those in flows of spherical particles.

Throughout this paper we consider only the simplest hard-disk potential interactions among the proteins. Deviations from this distribution will cause a small change in the short-time mobility of the proteins. However, the largest effects of the interaction potentials are likely to occur in the long-time diffusivity and some estimates of these

effects may be obtained from the work of Abney, Scalettar & Owicki (1989). These investigators found that for interaction potentials thought to be relevant in biological systems, the thermodynamic effects on the long-time diffusivity were close to those predicted by a hard-disk model. It is important to note that whereas many proteins and lipids are charged, the Debye screening length in cellular media (0.15 M NaCl solution) is about 8 Å and is smaller than the protein diameter.

The organization of the paper is as follows. Section 2 gives an outline of the simulation technique. Section 3 gives results for rotational as well as translational short-time self- and collective-mobilities of proteins in reconstituted membranes. This includes the aforementioned method for converting results obtained from purely two-dimensional simulations to those valid for three-dimensional membrane/aqueous-phase systems and comparison of the numerical results with those obtained from the effective-medium approximations due to Bussell *et al.* (1994, 1995*a*) and with the experimental results for various protein–membrane systems available in the literature. Section 4 gives the corresponding results for plasma membranes, while §5 summarizes the important findings of the work.

2. The numerical technique

As in most other simulations, we shall make use of the periodic boundary conditions for simulating homogeneous infinitely extended suspensions with a finite number of particles. Since the viscosity of the aqueous phase is much smaller than that of the lipid phase, it will suffice to consider purely two-dimensional disturbances in determining the influence of hydrodynamic interactions between disks separated by a distance comparable to the radii of proteins. Thus, we consider Stokes flow around N_p disks placed within a unit cell of a periodic array. It is convenient to express the velocity field in terms a streamfunction ψ defined by

$$u_1 = \partial\psi/\partial x_2, \quad u_2 = -\partial\psi/\partial x_1, \tag{5}$$

where u_1 and u_2 are velocity components along x_1- and x_2-axes. Since for Stokes flow the streamfunction satisfies the biharmonic equation $\nabla^4\psi = 0$, it can be shown that its solution can be expressed in terms of an integral equation

$$\psi(\boldsymbol{x}) = \psi_\infty(\boldsymbol{x}) + \frac{1}{4\pi\mu}\sum_{\alpha=1}^{N_p}\int_{C^\alpha}\left[f_2(\boldsymbol{y})\frac{\partial}{\partial x_1} - f_1(\boldsymbol{y})\frac{\partial}{\partial x_2}\right]S_2(\boldsymbol{x}-\boldsymbol{y})\,\mathrm{d}l_y, \tag{6}$$

where C^α denotes the perimeter of disk α, $\boldsymbol{f}$ the traction exerted by the fluid at point $\boldsymbol{y}$ on C^α, ψ_∞ is the streamfunction corresponding to the average velocity of the suspension, and S_2 is the spatially periodic Green's function for the biharmonic equation (Hasimoto 1959), i.e. S_2 is a solution of

$$\nabla^4 S_2(\boldsymbol{x}) = 4\pi[\tau^{-1} - \sum_{\boldsymbol{x}_L}\delta(\boldsymbol{x}-\boldsymbol{x}_L)], \tag{7}$$

where $\boldsymbol{x}_L$ are the lattice vectors of the periodic array and τ is the area of the unit cell. This choice of Green's function ensures that the velocity field automatically satisfies the condition of periodicity and that the average velocity of the suspension can be related in a simple manner to ψ_∞. As shown by Hasimoto (1959), S_2 is given by

$$S_2(\boldsymbol{x}) = -\frac{1}{4\pi^3\tau}\sum_{\boldsymbol{k}\neq 0} k^{-4}\exp(2\pi\mathrm{i}\boldsymbol{k}\cdot\boldsymbol{x}), \tag{8}$$

where $\boldsymbol{k}$ are the reciprocal space lattice vectors. It may be noted that while there is no Green's function for the biharmonic equation in an unbounded two-dimensional space, a Green's function does exist for the bounded periodic domains considered in the present study.

Now the usual method of multipole expansion consists of expanding the integrand in (6) in a Taylor series around the centre $\boldsymbol{x}^\alpha$ of particle α and expressing thereby the velocity or streamfunction in terms of force multipoles at the centre of the particle. The strengths of multipoles are subsequently determined from the boundary conditions at the surface of the particles (see, for example, Ladd 1988, 1989; Sangani & Yao 1988; Mo & Sangani 1994). This straightforward method turns out to be quite inefficient in resolving short-range lubrication forces in concentrated suspensions. For this purpose, it is advantageous instead to follow the method of dual multipole expansion outlined in Sangani & Mo (1994). According to this method the traction $\boldsymbol{f}$ on the surface of the particles is first decomposed into two parts: $\boldsymbol{f} = \boldsymbol{f}^{lub} + \hat{\boldsymbol{f}}$, where $\boldsymbol{f}^{lub}$ is the lubrication force localized on the surface of the particle to the narrow gaps between the particle and its neighbours while $\hat{\boldsymbol{f}}$ is the remainder force density which is more or less uniformly distributed throughout the surface of the particle. The lubrication force density is written explicitly in terms of the velocities of the particles and its contribution to the integral in (6) is expressed in terms of lubrication force multipoles centred in the narrow gap between the particles. Thus, for example, writing $\psi = \psi^{lub} + \hat{\psi}$, and expanding the right-hand side of (6) in a Taylor series, we obtain

$$\psi^{lub}(\boldsymbol{x}) \equiv \frac{1}{4\pi\mu} \sum_{\alpha\gamma} \int_{C^{\alpha+\gamma}} [\boldsymbol{t} f_z^{lub}(\boldsymbol{y}) - \boldsymbol{n} f_x^{lub}(\boldsymbol{y})] \cdot \boldsymbol{\nabla} S_2(\boldsymbol{x}-\boldsymbol{y})\, \mathrm{d}l_y$$

$$= \sum_{\alpha\gamma} \sum_{n=1}^{\infty} \boldsymbol{A}_{(n)}^{\alpha\gamma} (\cdot)^n \boldsymbol{\nabla}^{(n)} S_2(\boldsymbol{x}-\boldsymbol{x}_c^{\alpha\gamma}), \tag{9}$$

where $\alpha\gamma$ represents a pair of adjacent particles, $\boldsymbol{n}$ is the unit normal vector along $\boldsymbol{x}^\gamma - \boldsymbol{x}^\alpha$, $\boldsymbol{t}$ is the unit tangent vector in the gap with $\boldsymbol{n}\cdot\boldsymbol{t} = 0$, f_z^{lub} and f_x^{lub} are the components of lubrication forces along $\boldsymbol{n}$ and $\boldsymbol{t}$ respectively $\boldsymbol{x}_c^{\alpha\gamma} = \frac{1}{2}(\boldsymbol{x}^\alpha + \boldsymbol{x}^\gamma)$ is the centre of the gap, $C^{\alpha+\gamma}$ represents small segments of disks α and γ in the gap region where $\boldsymbol{f}^{lub}$ is taken to be non-zero, $\boldsymbol{\nabla}^{(n)} = \boldsymbol{\nabla}\boldsymbol{\nabla}\ldots$ denotes the nth-order gradient, $(\cdot)^n$ denotes an n-folder inner product, and $\boldsymbol{A}_{(n)}^{\alpha\gamma}$ is the nth-order lubrication force multipole defined by

$$\boldsymbol{A}_{(n)}^{\alpha\gamma} = \frac{1}{4\pi\mu} \frac{1}{(n-1)!} \int_{C^{\alpha+\gamma}} \mathrm{d}l_y (\boldsymbol{x}_c^{\alpha\gamma} - \boldsymbol{y})^{(n-1)} [\boldsymbol{t} f_z^{lub}(\boldsymbol{y}) - \boldsymbol{n} f_x^{lub}(\boldsymbol{y})]. \tag{10}$$

These multipoles can be expressed in terms of translational and rotational velocities of particles α and γ through a detailed analysis of the flow in the gap between the disks as shown in the Appendix.

The other part of ψ is written in terms of force multipoles at the centre of particles as in Sangani & Yao (1988):

$$\hat{\psi}(\boldsymbol{x}) = \psi_\infty(\boldsymbol{x}) + \sum_{\alpha=1}^{N_p} \left[B_0^\alpha \nabla^2 + \sum_{n=1}^{\infty} \left\{ (A_n^\alpha + B_n^\alpha \nabla^2) \frac{\partial}{\partial x_1} + (\tilde{A}_n^\alpha + \tilde{B}_n^\alpha \nabla^2) \frac{\partial}{\partial x_2} \right\} \frac{\partial^{n-1}}{\partial x_1^{n-1}} \right] S_2(\boldsymbol{x}-\boldsymbol{x}^\alpha). \tag{11}$$

The higher-order derivatives of S_2 with respect to x_2 need not be included in the above expression as they can be expressed as linear combinations of the terms included in (11). To determine the strengths of multipoles A_n^α, etc. we expand ψ around the centre

of each particle in terms of trigonometric functions as in the regular multipole expansion method described in Sangani & Yao (1988). Application of boundary conditions on the perimeter of each disk and use of orthogonality of the trigonometric functions yield an infinite set of equations. This set is truncated by neglecting the coefficients in (11) with n greater than a pre-selected value N_s to yield a total of $(4N_s+1)\,N_p$ multipole coefficients in an equal number of equations. In addition, there are $3N_p$ equations specifying the force and torque on each disk and $3N_p$ corresponding unknown translational and rotational velocity components of each disk.

The evaluation of the velocity due to lubrication force multipoles requires specifying the order to which the lubrication expansion is carried out and the region over which the non-zero lubrication forces apply as a function of the gap width between the adjacent particles. These were determined through a careful comparison with selected test problems as in Sangani & Mo (1994). With these parameters fixed from the test problems, it was found that the numerical results obtained using the regular force multipoles up to octupoles ($N_s = 4$) and lubrication force-multipoles up to quadrupoles ($n = 3$) were accurate to within 5% at all area fractions of disks for a wide variety of problems for which the exact solution was either available from the literature or could be determined to a high precision using the regular multipole expansion method with a sufficiently high N_s.

In what follows, we shall present the results for translational and rotational mobilities. These were obtained by averaging over several (10^2–10^3) configurations of hard disks obtained from a Monte Carlo code in which the disks initially placed on a square lattice are given random displacements; a new configuration of the disks is generated when the disks are non-overlapping. The self-mobilities required specifying a non-zero force or torque on a single particle and determining its translational and rotational velocity. This was conveniently accomplished by first inverting the matrix corresponding to the aforementioned set of $4(N_s+1)\,N_p$ equations. The collective mobility, which is the average velocity of the particles when a unit force is exerted on each of the particles, was determined by solving for the equations directly without inversion. We also need to determine the effective viscosity of the suspensions of disks in order to renormalize our mobility results for two-dimensional periodic suspensions to account for the aqueous phase viscous drag. This was done by imposing a linear shear flow and determining the average stresslet induced by the presence of the disks. The stresslet is given by

$$S_{ij}^{\alpha} = \frac{1}{2}\int_{C^{\alpha}} \{r_i f_j + r_j f_i - \tfrac{2}{3}\delta_{ij} r_k f_k - \mu(u_i n_j + u_j n_i - \tfrac{2}{3}\delta_{ij} u_k n_k)\}\,\mathrm{d}l_y, \tag{12}$$

where $\boldsymbol{y}$ is a point on the perimeter of the disk, $\boldsymbol{r} = \boldsymbol{y} - \boldsymbol{x}^{\alpha}$, and $\boldsymbol{n}$ is the unit outward normal at $\boldsymbol{y}$. The force $\boldsymbol{F}^{\alpha}$, stresslet $\boldsymbol{S}^{\alpha}$, and torque $\boldsymbol{L}^{\alpha}$ can be evaluated by combining the contributions from the regular multipole expansion terms (cf. (11)) and the lubrication force density. The latter can be evaluated from the expressions given in Appendix while the former is evaluated from

$$\hat{F}_1^{\alpha} = -4\pi\mu\tilde{A}_1^{\alpha}, \quad \hat{F}_2^{\alpha} = 4\pi\mu A_1^{\alpha}, \quad \hat{L}^{\alpha} = -4\pi\mu(2B_0^{\alpha} + A_2^{\alpha})\,\boldsymbol{e}_3, \tag{13}$$

$$\hat{S}_{11}^{\alpha} = -\hat{S}_{22}^{\alpha} = 2\pi\mu\tilde{A}_2^{\alpha}, \quad \hat{S}_{12}^{\alpha} = \hat{S}_{21}^{\alpha} = -2\pi\mu A_2^{\alpha}, \tag{14}$$

where $\boldsymbol{e}_3$ is the unit vector along the x_3-axis.

3. Reconstituted membranes

3.1. *Short-time self-diffusivity*

First we consider reconstituted membranes in which all proteins may be regarded as mobile. The computed short-time self-diffusivity $D_{s,c}$ for three different area fractions of disks is shown in figure 2.

Each point in figure 2 was obtained by averaging over several independent configurations of hard disks until the standard error in the mean over different configurations was within about 5%. As can be seen from this figure the computed diffusivity increases with the number of disks. The solid curves in the figure represent a logarithmic fit,

$$D_{s,c} = \frac{k_B T}{\mu h}[c_1 \log N_p + c_2], \tag{15}$$

to the computed diffusivities, and c_1 and c_2 as functions of ϕ are given in table 1.

It is clear from figure 2 that the computed diffusivity diverges logarithmically with the number of disks. This divergence can be explained in terms of an effective-medium theory. On a lengthscale large compared with a, the suspension appears as a continuum with an effective viscosity μ^*, and, therefore, on this large scale we are simulating the motion of a single particle in a two-dimensional periodic array with the surrounding-medium viscosity μ^*. The diffusivity of a single disk in a periodic cell with a square lattice of width $H(H \gg a)$ and the fluid viscosity μ^* can be determined readily from the analysis of Hasimoto (1959) to be given by

$$D_{per}(\mu^*) = \frac{k_B T}{4\pi h \mu^*}[\log(H/a) - 1.3105] = \frac{k_B T}{8\pi h \mu^*}[\log N_p - \log\phi - 1.4763], \tag{16}$$

where we have substituted $H^2/a^2 = \pi N_p/\phi$ to express the influence of periodic boundary conditions in terms of the number of disks used in the simulation. Since $D_{s,c}$ and $D_{per}(\mu^*)$ must have exactly same divergent behaviour in the limit $N_p \to \infty$, we see at once from (15) and (16) that

$$c_1(\phi) = \mu/(8\pi\mu^*). \tag{17}$$

Table 1 shows a comparison of the effective viscosity of the suspension derived from the above expression with the values of c_1 determined from the logarithmic fit of curves in figure 2 against the values determined from direct calculation of the effective viscosity by imposing a linear velocity gradient across the suspension and determining the average stresslet induced by the disks. The latter calculations for μ^* were found to be relatively insensitive to N_p. The fact that the effective viscosities determined by the two different methods are in agreement validates the use of the effective-medium theory to predict the influence of the periodic boundary conditions on computed diffusivities. Table 1 also gives the values of effective viscosity as determined from the $O(\phi)$ asymptote (Brady 1984)

$$\mu^* = \mu[1 + 2\phi + O(\phi^2)]. \tag{18}$$

We see that this asymptote gives significantly lower values for $\phi \geqslant 0.1$, indicating the strong influence of lubrication forces at higher area fractions.

To obtain estimates of the diffusivities of proteins in reconstituted membranes from the results of our two-dimensional simulations, we must account for the viscous resistance of the aqueous phase. To accomplish this, we view this as a problem in matched asymptotic expansions. In the inner region of scale a from the centre of a

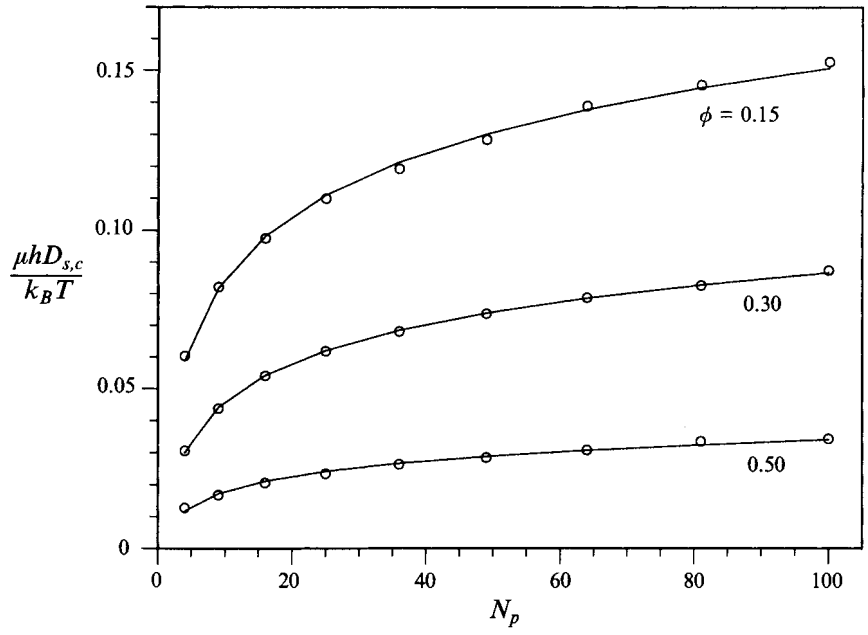

FIGURE 2. The computed short-time self-translational diffusivity $D_{s,c}$ as a function of the number of disks N_p for several values of disk area fraction ϕ. The circles represent the simulation results while the solid lines represent the logarithmic fit.

ϕ	c_1	c_2	(μ^*/μ)†	(μ^*/μ)‡	(μ^*/μ)‖
0.05	0.0352	0.0600	1.13	—	1.10
0.10	0.0312	0.0343	1.28	—	1.20
0.15	0.0285	0.0193	1.40	1.4	1.30
0.20	0.0238	0.0140	1.67	—	1.40
0.25	0.0204	0.0096	1.95	—	1.50
0.30	0.0175	0.0057	2.27	2.2	1.60
0.40	0.0116	0.0027	3.42	—	—
0.50	0.0069	0.0021	5.77	5.4	—
0.60	0.0031	0.0026	13.0	—	—

† Calculated from $1/8\pi c_1$ (cf. (17)).
‡ Calculated from average stresslet in sheared suspensions.
‖ Calculated using the $O(\phi)$ asymptote (18) (Brady 1984).

TABLE 1. The coefficients c_1 and c_2 in the logarithmic fit of computed self-diffusivity (cf. (15)) and a comparison of the effective viscosity obtained from various methods

forced disk the hydrodynamic interactions between disks are governed to leading order by two-dimensional Stokes flow interactions and are thus adequately captured by our simulation. In the outer region of scale λa, however, the aqueous-phase resistance and the three-dimensional nature of the disturbances are important as in Saffman's (1976) analysis while our computed results are influenced by the periodic boundary condition. Fortunately, the discrete nature of the suspension is unimportant on this outer lengthscale and we can treat the membrane as simply a two-dimensional Newtonian fluid with an effective viscosity μ^*. Thus to obtain the correct expression for the diffusivity in the membrane–aqueous-phase system, we must subtract from our

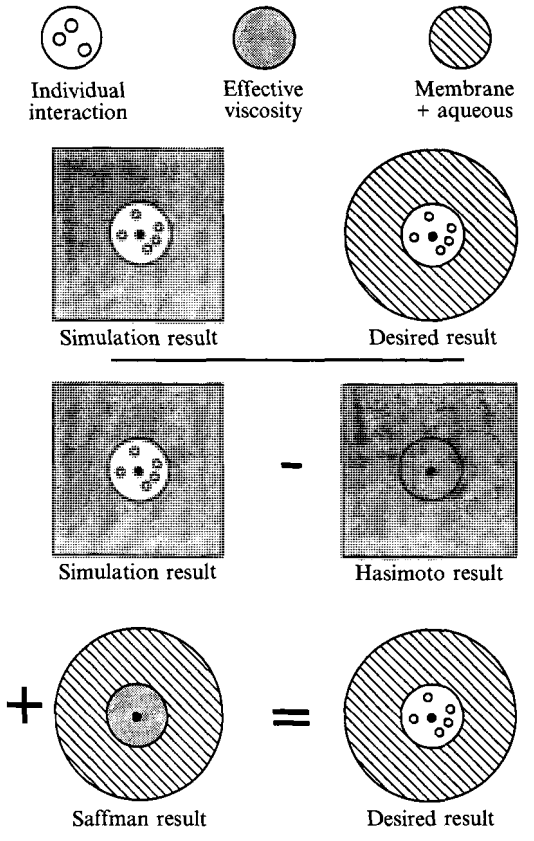

FIGURE 3. A schematic representation of the outer-region correction to self-diffusivity. The discrete nature of the suspension in the inner region is indicated by a circle enclosing a number of disks (open circles) around a forced disk (filled circle). The outer region with periodic boundary conditions is denoted by a shaded square while the unbounded outer region with aqueous-phase viscous resistance is denoted by a hatched region inside a large circle.

computed diffusivity the contribution due to an outer region consisting of periodic two-dimensional suspension and add instead the contribution from the outer region for the membrane–aqueous-phase system. The latter is obtained simply by replacing μ in (3) with μ^* and λ with

$$\lambda^* = (\mu^*/\mu)\lambda = \mu^* a/(\mu' h). \tag{19}$$

Thus, the short-time self-diffusivity D_s is related to our computed diffusivity by

$$D_s = D_{s,c} - D_{per}(\mu^*) + D_0(\mu^*) = \frac{k_B T}{\mu h}[c_2(\phi) + c_1(\phi)(2\log\lambda^* + \log\phi + 0.3218)]. \tag{20}$$

Figure 3 illustrates schematically the method for estimating diffusivities in reconstituted membranes. The inner region near a forced disk is indicated by a discrete suspension of disks while the outer region in computations corresponds to an effective periodic medium indicated by a shaded region. The outer region in the aqueous-phase–membrane system is indicated by a hatched region. Note that the inner region in determining both D_{per} and D_0 corresponds to a suspending medium of viscosity μ^* while the actual viscosity is the lipid viscosity μ. This incorrect viscosity, however, does not affect the final result since the difference $D_{per} - D_0(\lambda^*)$ is independent of the choice of viscosity in the inner region.

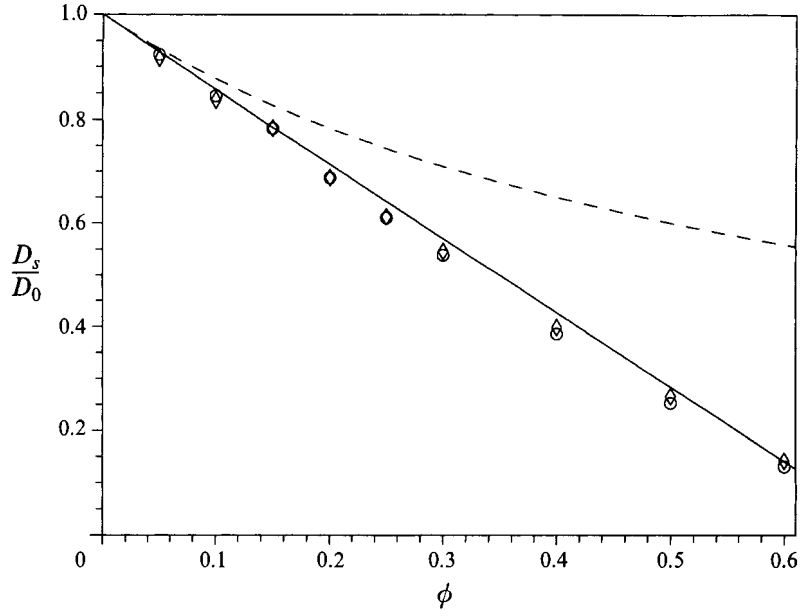

FIGURE 4. A comparison of the computed short-time self-diffusivity with various theories. The simulation results are indicated by circles, the dilute asymptote (21) due to Bussell *et al.* (1994) by the solid line, the effective-medium approximation (22) with the dilute asymptote $\mu^* = \mu(1+2\phi)$ by the dashed line, and the effective-medium approximation with the computed values of μ^* (cf. table 1) is shown by diamonds.

We now compare the simulation results to the analytical results of Bussell *et al.* (1994). For low area fractions these investigators obtained

$$\frac{D_s}{D_0(\lambda)} = 1-2\phi\left[1-\frac{1+\log 2-9/32}{\log\lambda-\gamma}+\bar{\mathscr{R}}\right], \tag{21}$$

where $\bar{\mathscr{R}}$, a remainder arising from higher-order reflections in two-particle interaction calculations, had a negligibly small numerical value of $O(10^{-3})$. Figure 4 shows a comparison of this low-ϕ asymptote with the computed diffusivities for $\lambda = 250$, a typical value for proteins in reconstituted membranes. The asymptote is seen to give remarkably accurate values of diffusivities at all area fractions.

For estimating diffusivities in non-dilute suspensions, Bussell *et al.* (1994) used an effective-medium theory approximation to arrive at the following estimate:

$$D_s = \frac{k_B T}{4\pi h\mu^*}\left[\log\lambda^*-\gamma+\left(\frac{\mu^*}{\mu}-1\right)\left\{\log 2-\frac{9\mu^*}{15\mu^*+17\mu}\right\}\right], \tag{22}$$

with $\mu^* = \mu(1+2\phi)$ based on the low-area-fraction asymptote. As seen in figure 4, this significantly overpredicts the diffusivity at most area fractions. If, however, one uses the actual values of μ^*/μ obtained from simulations (cf. fourth column of table 1), then a very good agreement is found between the computed diffusivities and the effective-medium approximation given by (22). In other words, the use of an effective-medium approximation with an enhanced viscosity to describe the effect of protein interactions on the self-diffusivity works well provided that one uses the actual effective viscosity of the non-dilute suspension.

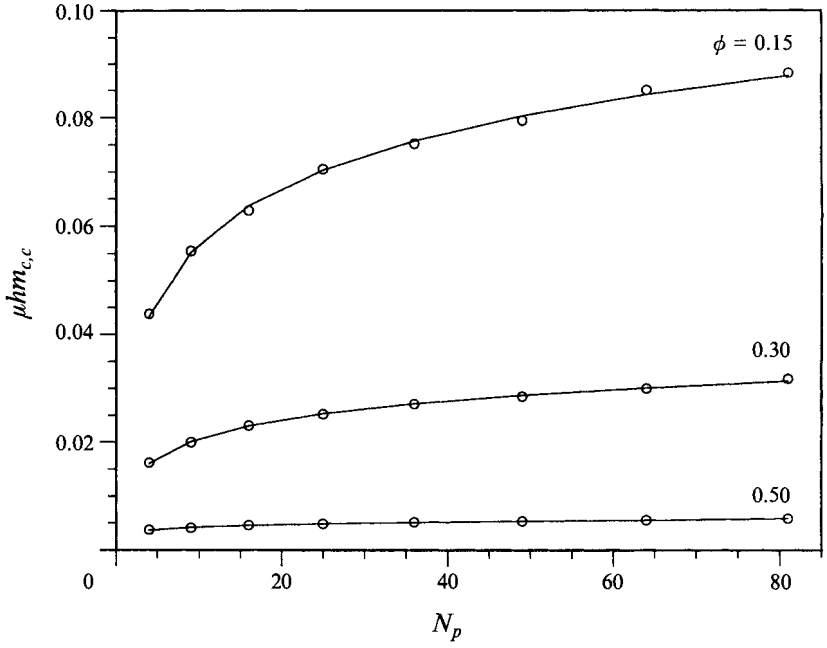

FIGURE 5. The computed values of collective mobility as a function of the number N_p of disks for several indicated values of ϕ.

3.2. *Collective mobility*

We now present results for the average mobility m_c of the disks when all the disks in the suspension are acted upon by an equal force. This calculation is relevant to determining gradient diffusivity D_g when the area fraction of protein is slowly varying in the plane of the membrane. Thus, for example, the gradient diffusivity can be computed from the collective mobility m_c by (Batchelor 1976)

$$D_g = m_c\left[\frac{\phi}{1-\phi}\left(\frac{\partial\tilde{\mu}}{\partial\phi}\right)_{p,T}\right], \tag{23}$$

where $\tilde{\mu}$ is the chemical potential and p is the pressure. As noted by Kops-Werkhoven & Fijnaut (1981) and Kops-Werkhoven, Vrij & Lekkerkerker (1983), the quantity inside the square bracket in the above expression equals $k_B T/S(\mathbf{0})$, where $S(\mathbf{0})$ (cf. (25) and (28)) is the zero-wavenumber limit of the structure factor of the suspension at equilibrium.

Figure 5 shows the computed short-time collective mobility $m_{c,c}$ as a function of N_p for several different area fractions of disks. As in the case of self-mobility, the solid curves are the logarithmic fit

$$m_{c,c} = \frac{1}{\mu h}[c_3 \log N_p + c_4] \tag{24}$$

to the computed values, and c_3 and c_4 are listed in table 2. To obtain the collective mobility in the membrane–aqueous-phase system, we follow the argument used in determining self-mobility. Thus, we subtract the collective mobility for an effective periodic medium from the computed mobility and add the corresponding contribution from a membrane with an enhanced viscosity in contact with the aqueous phase. In the present case, however, we must also account for the fact that there are forces acting on

ϕ	c_3	c_4	$S(\mathbf{0})$†	$S(\mathbf{0})$‡	μhm_c‖	μhm_c¶	μhm_c*
0.15	0.01473	0.01333	0.531	0.518	0.172	0.074	0.162
0.30	0.00504	0.00452	0.258	0.288	0.062	−ve	0.064
0.50	0.00068	0.00056	0.081	0.099	0.0120	−ve	0.0115

† From Padé approximant (24) due to Chae *et al.* (1969).
‡ From computed values of c_3 and c_1 (cf. table 1) with the use of (26).
‖ From simulations and (27) with $\lambda = 250$.
¶ Dilute asymptote (29) (Bussell *et al.* 1994).
* Effective-medium approximation (31).

TABLE 2. The coefficients c_3 and c_4 in the logarithmic fit of computed collective mobility (cf. (24)), comparison of the structure factor $S(\mathbf{0})$ determined from c_3 and c_1 with the Padé approximant (28) by Chae *et al.* (1969), and an assessment of dilute and effective-medium approximations.

the neighbouring disks in addition to the force acting on the test disk. At large distances from the test disk, the disks give rise to a constant body force density which is balanced by the mean pressure gradient. Near the test disk, however, there is a net depletion of disks due to the area-exclusion effect which is accounted for by requiring that the flow induced by the test disk at large distances must correspond to that induced by a point force $\boldsymbol{F}^{ap}$ given by

$$\boldsymbol{F}^{ap} = n\boldsymbol{F}\int[g(\boldsymbol{r}\,|\,\mathbf{0})-1]\,\mathrm{d}\boldsymbol{r} = S(\mathbf{0})\,\boldsymbol{F}, \tag{25}$$

where $g(\boldsymbol{r}\,|\,\mathbf{0})$ is the pair probability density scaled by the number density n so that g approaches unity as $r\to\infty$, and $ng = \delta(\boldsymbol{r})$ for $r < 2a$. $S(\mathbf{0})$ is the zero-wavenumber limit of the structure factor whose values for the hard-disk spatial distribution are given by Chae, Ree & Ree (1969). The velocity due to the apparent force $\boldsymbol{F}^{ap}$ in the above expression can be thought of as the velocity induced by the discrete distribution of disks near the test disk, including the test disk, minus that induced by the uniform pressure gradient.

Thus, we see that, to correct for the aqueous phase resistance and the periodic boundary conditions, we simply need to multiply the self-mobility correction by the ratio of the apparent force to the actual force, or by $S(\mathbf{0})$. We therefore have $m_c = m_{c,c} + S(\mathbf{0})\,[m_0(\mu^*) - m_{per}(\mu^*)]$, or

$$c_3 = S(\mathbf{0})\,c_1 = S(\mathbf{0})\,\mu/(8\pi\mu^*) \tag{26}$$

and

$$\mu hm_c = c_4 + c_3[2\log\lambda^* + 0.3218 + \log\phi]. \tag{27}$$

Table 2 shows a comparison of $S(\mathbf{0})$ evaluated from the computed values of c_1 and c_3 with the Padé approximation for $S(\mathbf{0})$ given by Chae *et al.* (1969):

$$S(\mathbf{0}) = \frac{(1-1.9682\phi+0.9716\phi^2)^2}{1+0.0636\phi-0.5446\phi^2-0.4632\phi^3-0.1060\phi^4+0.0087\phi^5}. \tag{28}$$

The agreement is seen to be reasonably good. The table also gives the values of m_c for the special case of $\lambda = 250$ with which we shall compare the predictions of theory.

Bussell *et al.* (1994) have obtained an expression for the collective mobility in dilute suspensions. After correcting for a small algebraic error in their expression (68) for ${}^3U/U_0$ we find that

$$\frac{m_c}{m_0} = 1+\phi\left[-6+\frac{3\log 2-17/16+0.38}{\log\lambda-\gamma}\right] = 1+\phi\left[-6+\frac{1.40}{\log\lambda-\gamma}\right] \quad (\phi \ll 1), \tag{29}$$

where m_0 is the mobility at infinite dilution (cf. (3)). For $\lambda = 250$, the expression on the right-hand side of (29) reduces to $1-5.72\phi$. In contrast to what we found for self-mobility, the above asymptote for dilute suspensions grossly underpredicts the mobility at non-dilute area fractions (cf. table 2). Bussell *et al.* (1994) also gave another expression in which certain two-disk interaction calculations were multiplied by the radial distribution function g for a non-dilute hard-disk suspension. Using that expression yields $m_c = 0.078$ at $\phi = 0.15$, a slight improvement over that predicted by (29). At any rate, both of their expressions give unrealistic negative values for $\phi = 0.3$ and 0.5, and therefore it is desirable to formulate an alternative theory for predicting collective mobility in non-dilute suspensions.

Table 2 shows a comparison with the predictions of an effective-medium theory for the collective mobility. The agreement between the computed values and the theory is excellent in this case and hence we describe the theory briefly. In this theory we solve for Stokes flow past a disk of radius unity with the fluid viscosity equal to μ for $r < R$ and μ^* for $r > R$. In addition, a constant body force equal to nF is assumed to apply in the effective medium, $r > R$. As seen from within the effective medium, the net force on the test disk appears to be F minus the buoyancy force $\phi R^2 F$. Equating this apparent force to $FS(\mathbf{0})$ gives

$$R^2 = [1-S(\mathbf{0})]/\phi. \tag{30}$$

It may be noted that $S(\mathbf{0}) \to 1-4\phi$ as $\phi \to 0$, so that $R \to 2$ for dilute suspensions. For higher values of ϕ, R is smaller, e.g. $R = 1.36$ at $\phi = 0.5$. Now the continuity of the velocity and stress at $r = R$ together with the no-slip boundary condition at $r = 1$ and the matching requirement with Saffman's (1976) outer region accounting for the aqueous-phase viscous resistance yields

$$m_c = \frac{S(\mathbf{0})\,\mu}{4\pi h \mu^*}\left[\log\lambda^* - \gamma + A + \frac{\phi\mu^*}{S(\mathbf{0})\,\mu}B\right], \tag{31}$$

where

$$A = \frac{\mu^*-\mu}{\mu}\left[\log R - \tfrac{1}{2} + \tfrac{1}{2}R^{-2} + \frac{1}{4C\mu}\{2\mu^*(R^{-2}-R^{-4}) - (\mu^*-\mu)(1+R^{-4})(1-R^{-2})\}\right], \tag{32}$$

$$B = \log R - \tfrac{1}{2} + \tfrac{1}{2}R^{-2} - \frac{\mu^*-\mu}{4C\mu}(1-R^{-2})^3, \tag{33}$$

$$C = 1 + \frac{\mu^*-\mu}{2\mu}(1-R^{-4}). \tag{34}$$

For small ϕ, (31) compares well with the exact asymptote (29) with the coefficient 1.40 in the latter replaced by 1.14, while at high ϕ it predicts mobilities within 5% of the computed values.

It is interesting to note that our finding that the dilute asymptote for the collective mobility in the suspension of disks fails even at moderate values of ϕ is similar to the corresponding results for suspensions of spheres. For spheres, Brady & Durlofsky (1988) have constructed an effective-medium approximation in which the suspension viscosity is taken to be that of the suspending fluid. Such an approximation does not yield good estimates of mobility in the present case.

We might add here that the idea of using an effective-medium approximation for $r > R$ with R determined from the structure factor data (cf. (30)) could also be applied to estimate the self-diffusivity. The self-mobility can be estimated from (31) by

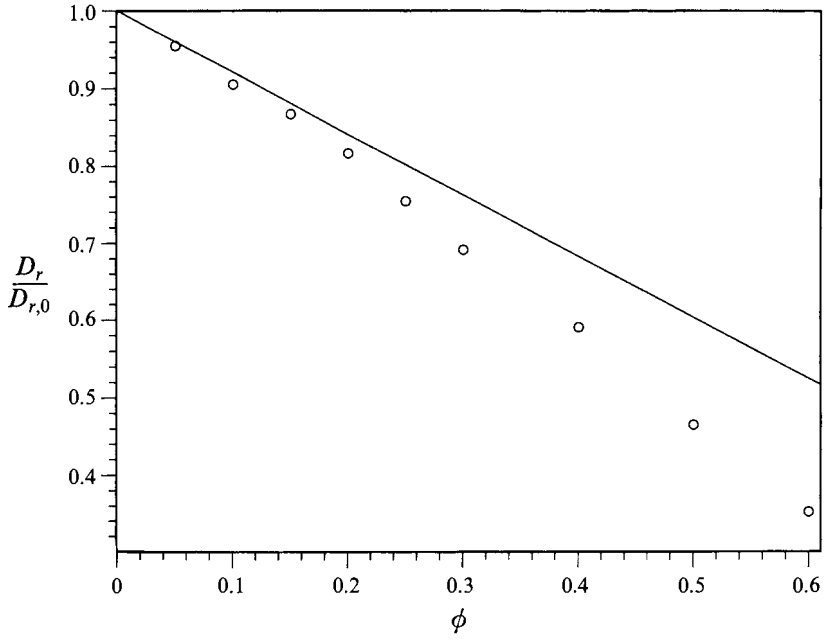

FIGURE 6. Rotational diffusivity as a function of ϕ. The circles are the simulation results while the solid line is the low-ϕ asymptote.

substituting $B = 0$ and $S(\mathbf{0}) = 1$ in that equation. The computed self-diffusivity ratio D_s/D_0 at $\lambda = 250$ at $\phi = 0.5$ is 0.252 while the effective-medium approximation computed with $R = 1.342$ determined from (30) gives 0.262. In comparison, the effective-medium approximation with $R = 2$ yields 0.281. The corresponding numbers for $\phi = 0.3$ are 0.537 (computed), 0.547 ($R = 1.54$), and 0.560 ($R = 2$). Thus, we see that while using a simpler approximation with $R = 2$ worked reasonably well in case of self-mobility, using variable R yields excellent estimates for both self- and collective mobilities.

3.3. *Rotational diffusivity*

Figure 6 shows results for rotational diffusivity. $D_{r,0}$ is the diffusivity at infinite dilution (cf. (4)). As mentioned in the Introduction, the velocity induced by a rotating disk, or a point torque, decays as $1/r$ in two-dimensional space, and therefore it is unnecessary to account for the viscous resistance of the aqueous phase. The results for rotational diffusivity were found to be relatively insensitive to N_p.

The solid line in figure 6 corresponds to the dilute asymptote

$$m_r = m_{r,0}(1-0.793\phi) \tag{35}$$

obtained from a pair-interaction calculation using

$$m_r = m_{r,0} + n\int_{r>2a} [m_r(\mathbf{0}\,|\,\boldsymbol{r}) - m_{r,0}]\,\mathrm{d}\boldsymbol{r}, \tag{36}$$

where $m_r(\mathbf{0}\,|\,\boldsymbol{r})$, the rotational mobility of the disk at the origin given the presence of a force and torque free disk at $\boldsymbol{r}$, is calculated in Bussell *et al.* (1992). We see that the dilute asymptote gives estimates accurate to within 10% for $\phi < 0.3$. An effective-medium approximation in which the suspension for $r > 2a$ is treated as a fluid of viscosity μ^*, being considerably greater than the exact results or the dilute-theory asymptote, does not yield accurate estimates of the rotational mobility.

We note that the rotational mobility is not as hindered because of hydrodynamic interactions as the self- and collective mobilities. The rotational mobility is reduced by a factor of roughly 3 as ϕ is varied from zero to 0.6 while the translational mobilities decreased by a factor of 10.

3.4. *Comparison with experiments*

Several different techniques have been developed for measuring rotational and translational diffusivities of proteins. Perhaps one of the earliest, and by far the most reliable one, is the technique of fluorescent photobleaching and recovery (Axelrod *et al.* 1976) which measures the fluorescent recovery of a photobleached area due to diffusion of proteins from the surrounding region in the membrane. The timescale for diffusion in these experiments is much greater than the time it takes for the spatial configuration of disks to change appreciably and thus these experiments measure the long-time self-diffusivity whereas we have computed the short-time diffusivity. The long-time diffusivity can be determined, in principle, with the help of the Langevin equation using Stokesian dynamics to account for hydrodynamic interactions by the method outlined by Ermak & McCammon (1978) and refined over recent years by Brady & Bossis (1988). However, this will require substantially more computational effort and therefore we leave it to a future investigation. In what follows, we shall use an approximate scheme for estimating long-time diffusivities from the short-time values obtained in the present study.

The long-time diffusivity is generally much smaller than the short-time diffusivity because of thermodynamic effects such as the volume exclusion and the inter-particle non-hydrodynamic forces. The thermodynamic contribution to long-time diffusivity can be estimated using simulations in which the hydrodynamic mobilities of the individual particles are treated as independent of the spatial configurations of particles. Taking the mobility to be the same as the short-time mobility averaged over several configurations, we approximate the long-time diffusivity as

$$D_l = fD_s, \tag{37}$$

where f is determined as a function of ϕ through suitable simulations of the long-time diffusivity with the short-time diffusivity of the individual particles taken as unity. Medina-Noyala (1988) has studied the validity of the above approximate scheme for the suspension of spheres and found it to yield very good agreement with the experimental results for diffusivities of spheres. Recently, Brady (1994) showed that (37) can be derived formally using a self-consistent closure of the N-particle Smoluchowski equation.

The thermodynamic correction factor f can be estimated either through non-hydrodynamic Brownian or Monte-Carlo simulations or through a suitable analytic approximation such as one suggested by the caging theory due to Rallison (1988). Bussell *et al.* (1995*a*) applied both of these techniques and found a good agreement between them. They also found good agreement between the experimentally determined long-time self-diffusivity and that predicted by (37) with D_s determined for dilute suspensions (cf. (21)). Their calculations used the simulations of hard hexagonal disks on a triangular lattice with no hydrodynamic interactions by Saxton (1987) who gave

$$f = 1 - 2.1187\phi + 1.8025\phi^2 - 1.6304\phi^3 + 0.9466\phi^4 \tag{38}$$

as a fit to numerical simulation results for ϕ up to 0.65.

We now compare our theory with the experimental results of Peters & Cherry (1982) and Chazotte & Hackenbrock (1988) who measured long-time self-diffusivities of

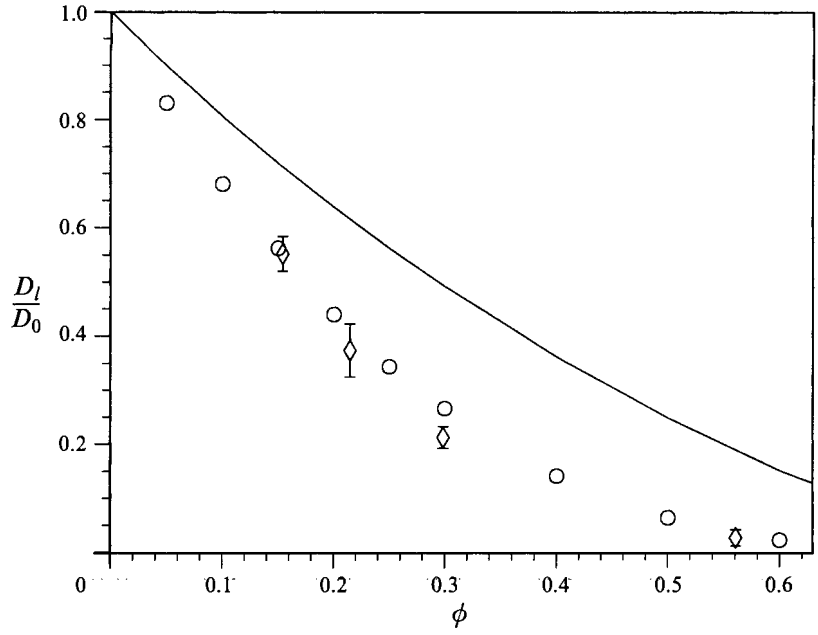

FIGURE 7. A comparison of the theory (open circles) for the long-time self-diffusivity with the experimental data (diamonds) of Peters & Cherry (1982) for diffusivity of bacteriorhodpsin in a reconstituted lipid bilayer. D_0 is chosen such that the theory and experiments match exactly at the lowest area fraction. The solid line indicates the thermodynamic effect represented by function f in (38) (Saxton 1987).

bacteriorhodopsin and complex III, respectively. (Both bacteriorhodopsin and complex III are integral membrane proteins.) In making these comparisons, we need to estimate the protein area fraction ϕ, the height h of the bilipid layer, the radius a of the protein molecules, and the viscosity μ of the lipid phase. Most of these parameters are estimated from various sources available in the literature while the others have to be estimated assuming such quantities as the fraction of protein mass that lies inside the lipid bilayer. For example, for bacteriorhodopsin experiments we take $a = 2$ nm, $\mu = 1$ P, $h = 5$ nm, and $\mu' = 0.01$ P from Peters & Cherry (1982) which yields $\lambda = 250$ while we choose $\lambda = 750$ for complex III experiments on the basis that at very dilute concentrations the diffusivity of complex III is three times smaller than that of bacteriorhodopsin. In other words, we assume the viscosity μ to be three times larger. The area fraction is estimated from the crystal radii of protein and lipid molecules which are available from other sources (e.g. Henderson & Unwin 1975) and the mass fraction of protein in the membrane. Further details on estimating various parameters may be found from Bussell *et al.* (1995*a*). It is important to emphasize that all parameters required for comparison are estimated *a priori* from sources independent of the experimental data with which we shall make the comparison, except for some cases in which we used the diffusion data available at the lowest value of ϕ to adjust a single undetermined parameter in estimating the infinite-dilution diffusivity D_0. This is justified since our main goal in the present study is to assess the concentration dependence of the diffusivity. The same will apply to the comparison with the experimental values of diffusivity of proteins in cellular plasma membranes to be presented in §4.3.

Figure 7 shows a comparison with data for bacteriorhodopsin taken from Peters &

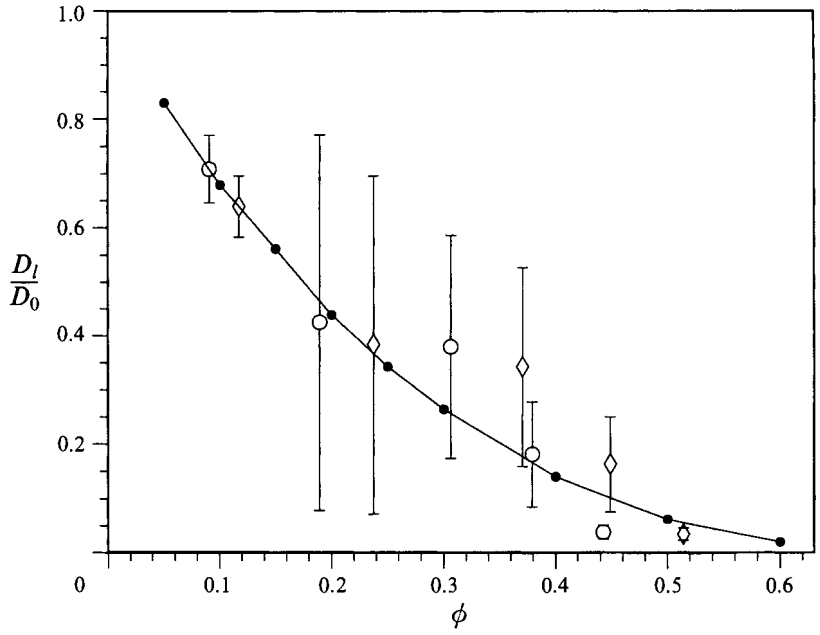

FIGURE 8. Comparison with the experimental data on complex III diffusivity in inner mitochondrial membranes from Chazotte & Hackenbrock (1988). Again, D_0 is chosen to match the experimental data at the lowest area fraction. The open circles represent the experimental data assuming a protein mass fraction residing in the membrane of 0.3 while the diamonds correspond to the mass fraction of 0.4. The theory is indicated by the solid line and filled circles.

Cherry (1982). The solid curve in that figure corresponds to f given by Saxton (1987) (cf. (38)) which represents the thermodynamic contribution to the long-time diffusivity. We note that both hydrodynamic and thermodynamic interactions must be accounted for to obtain good agreement between theory and experiments. Figure 8 shows the comparison with data for complex III diffusivity in inner mitochondrial membranes enriched with soybean phospholipids as given by Chazotte & Hackenbrock (1988). In both figures D_0 was adjusted so that its experimental value at the lowest area fraction ($\phi \approx 0.1$) matches the theory. Furthermore, it was also necessary to assume the value of the fraction of protein mass residing in the membrane to estimate ϕ. The data indicated by circles correspond to an assumed value of 0.3 for the fraction of protein mass while the diamonds correspond to an assumed value of 0.4. These values for the system are quoted by Deatherage, Henderson & Capaldi (1982) and Leonard, Haiker & Weiss (1987). The vertical bars representing experimental uncertainty indicate the inadequacy of these data for testing the theory except at high area fractions. At any rate, the theory is in reasonable agreement with the data.

Peters & Cherry (1982) have also presented data on the dependence of diffusivity on the aqueous-phase viscosity at $\phi = 0.154$. These data are compared with the theory in figure 9. D_0 for this figure is the same as that used in figure 7 as both correspond to the same area fraction of proteins. The good agreement in this case implies (i) the validity of the aqueous-phase viscous resistance screening suggested by Saffman even when λ is decreased from 250 to about 25; and (ii) a variation of D_l/D_0 as $f\mu/\mu^* \log \mu'$.

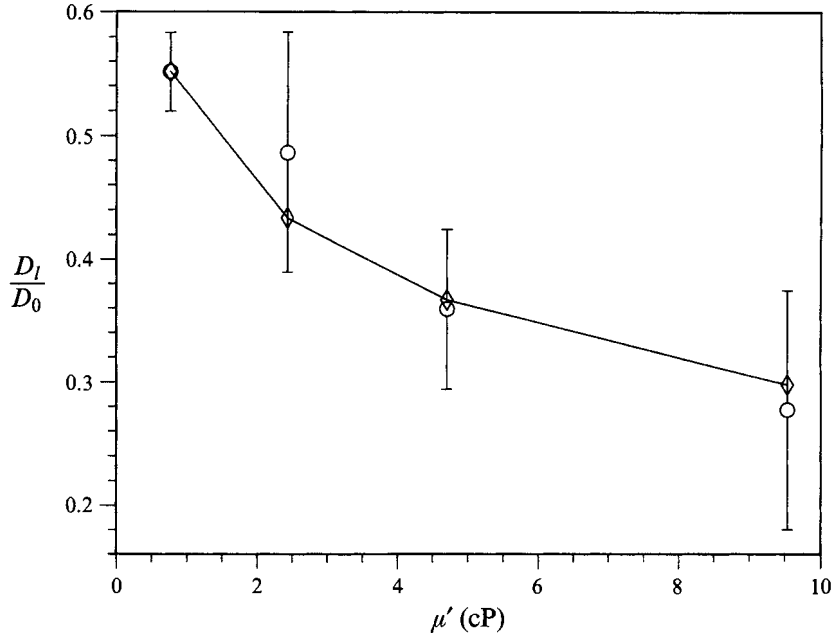

FIGURE 9. Comparison of theory and experiments for the dependence of the long-time diffusivity on the aqueous-phase viscosity. The circles are data for bacteriorhodpsin by Peters & Cherry (1988) and the diamonds are the computed results from theory. D_0 was chosen to be the same as in figure 7.

4. Plasma membranes

As mentioned in the Introduction, protein diffusivities in cellular plasma membranes are generally much smaller than in reconstituted membranes having the same area fraction of proteins. Four factors are generally thought to influence protein diffusivity in plasma membranes: area exclusion, hydrodynamic interactions, obstruction of protein motion due to interaction between the cytoplasmic tail of the protein and cytoskeleton structures, and transient binding (immobilization) of proteins. The purpose of our calculations is to assess the contribution of hydrodynamic interactions to diffusivity. As noted by Bussell *et al.* (1955*b*) hydrodynamic interactions will significantly slow the motion of mobile proteins because the presence of immobile proteins causes Brinkman screening of hydrodynamic disturbances induced by the mobile proteins. This Brinkman screening is more important than the Saffman screening. Accordingly, we shall consider in this section the diffusivities of mobile disks through a suspension in which a fraction of the disks are fixed. As in the previous section, we shall first compare the results of numerical simulations with dilute and effective-medium analytical results and then with experiments.

4.1. *Self-diffusivity*

The results for the short-time self-diffusivity as a function of N_p for several different combinations of the total area fraction ϕ_t and the immobilized-disk area fraction ϕ_i are shown in figure 10. As in previous calculations, each point in the figure represents an average over many (10^2–10^3) independent configurations of hard disks. In generating these configurations from an initially ordered arrangement by a Monte-Carlo procedure, we allowed all the disks to move. Thus the overall spatial configurations are the same as that for a free suspension of hard disks. It is only in doing hydrodynamic

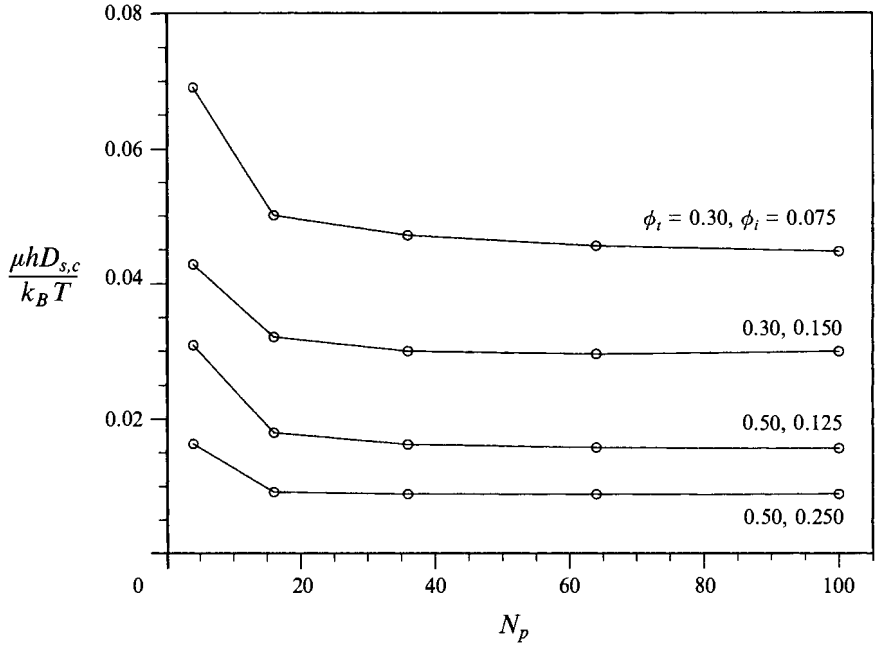

FIGURE 10. Short-time self-diffusivity as a function of N_p in partially fixed suspensions at several indicated values of the total area fraction ϕ_t and immobilized disk area fraction ϕ_i.

calculations that we take a fraction of the disks to be immobile. The self-diffusivity is seen to become nearly independent of N_p for $N_p > 40$. Thus we see that, unlike the case of free suspensions, the two-dimensional model is adequate for determining the diffusivities in partially fixed suspensions, and $D_s = D_{s,c}$. All subsequent calculations were made with $N_p = 100$.

Figure 11 gives the self-diffusivity as a function of the mobile area fraction ϕ_m for two different values of ϕ_i. The diffusivity varies linearly with ϕ_m over a substantially large range of area fractions. Thus we fit our computed results by a linear relation

$$\mu h D_s / k_B T = c_5(\phi_i) + \phi_m c_6(\phi_i) \tag{39}$$

and list c_5 and c_6 for several different ϕ_i in table 3. The diffusivity of a single mobile disk through a completely immobilized suspension ($\phi_m = 0$) is then given by $c_5 k_B T/\mu h$. The diffusivity for this limiting case is plotted in figure 12. We shall compare these results with the theory after a brief review of the latter.

Bussell *et al.* (1995*b*) were the first to suggest treating cellular plasma membranes as partially fixed beds of particles. They presented results for dilute fixed beds which we shall extend to higher area fractions. The presence of fixed particles introduces an additional term in the conditionally averaged momentum equation given the presence of a test disk at the origin (Brinkman 1947; Howells 1974; Hinch 1977). Thus, the momentum equation for flow around a test disk satisfies the Brinkman equation

$$-\nabla p + \mu \nabla^2 \boldsymbol{u} + \mu k^{-1} \boldsymbol{u} = \boldsymbol{0}, \tag{40}$$

where k is the Darcy permeability of a fixed bed with area fraction ϕ_i of fixed disks and μ is the viscosity of the medium. The values of k for hard-disk distributions have been obtained by Sangani & Yao (1988) in an earlier investigation with smaller N_p and more

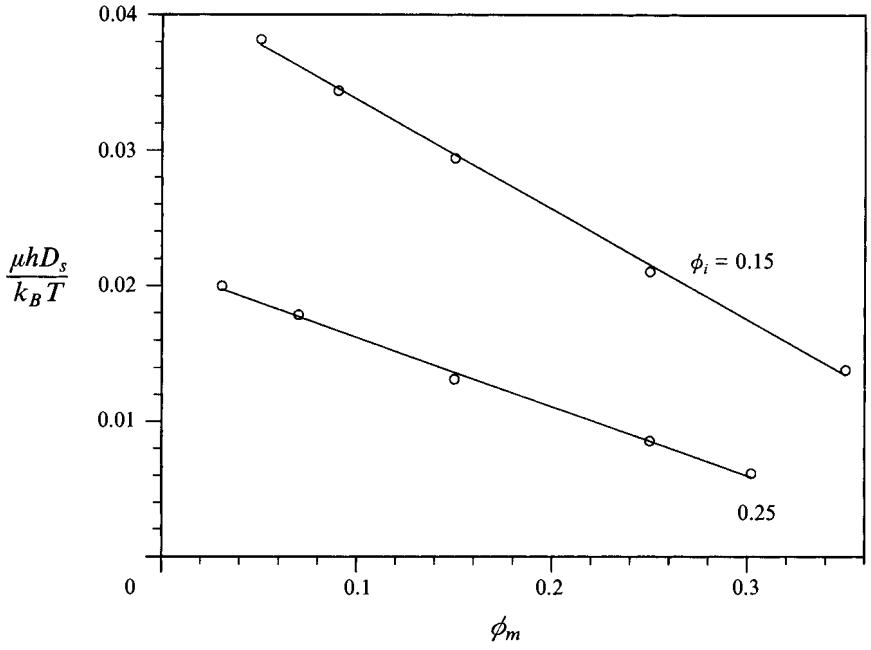

FIGURE 11. The short-time self-diffusivity as a function of ϕ_m for two different values of ϕ_i. The straight lines are the best fit to computed values.

ϕ_i	c_5	c_6	c_7	c_8
0.05	0.0918	−0.144	0.930	−1.00
0.10	0.0594	−0.104	0.847	−1.02
0.15	0.0418	−0.081	0.765	−0.93
0.20	0.0300	−0.064	0.725	−1.01
0.25	0.0213	−0.051	0.652	−0.95

TABLE 3. The coefficients c_5 and c_6 in the linear fit of self-diffusivity (cf. (39)) in partially fixed suspensions, and c_7 and c_8 in the linear fit of rotational diffusivity (cf. 45)).

accurately recently by Sangani & Mo (1994). These investigators determined the average force F exerted on the fixed disks by fluid moving with an average superficial velocity U. Denoting their results in terms of an average resistivity $\mathscr{R} = F/(4\pi\mu U)$, the permeability of a fixed bed with an area fraction ϕ_i is given by

$$k = a^2/(4\phi_i \mathscr{R}). \tag{41}$$

Howells (1974) obtained an estimate of $\mathscr{R}$ by solving for Brinkman flow (cf. (40)) around a fixed test disk and equating the force on the disk to $4\pi\mu U\mathscr{R}$ to obtain

$$\mathscr{R} = \frac{a^2}{2k} + \frac{a}{k^{1/2}} \frac{K_1(ak^{-1/2})}{K_0(ak^{-1/2})}, \tag{42}$$

where K_0 and K_1 are modified Bessel functions. According to this scheme, the effective-medium approximation is obtained by solving (41) and (42) simultaneously.

Now we can readily use the above result to obtain an approximation for the mobility of a single disk through a fixed bed by noting that the effective-medium theory does not

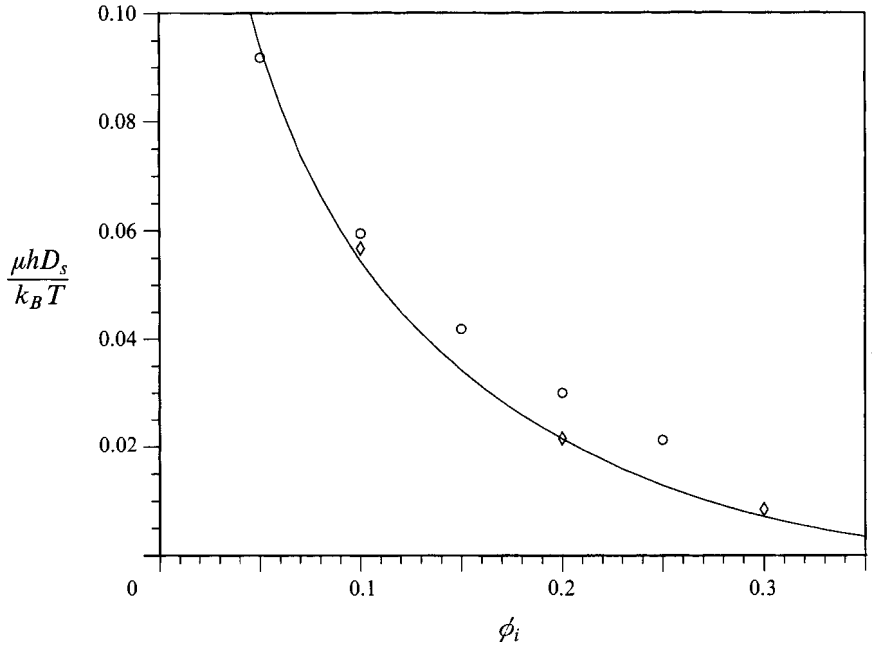

FIGURE 12. Comparison of the computed values (open circles) of D_s at $\phi_m = 0$ with the Brinkman approximation (solid line) given by (41)–(43). The diamonds are the computed values (Sangani & Mo 1994) of $1/4\pi\mathscr{R}$, $\mathscr{R}$ being the resistivity in the fixed bed.

distinguish between the disk moving through the fixed bed with a zero average velocity of the bed and the fluid moving through a completely fixed bed. Thus the effective-medium approximation for the mobility of a cylinder of height h is simply given by

$$m_s = (4\pi\mu h\mathscr{R})^{-1}. \tag{43}$$

The solid line in figure 12 represents results for the self-mobility of a disk as a function of ϕ_i obtained by solving (41)–(43). The agreement between the theory and simulation results obtained using the values of c_5 in table 3 is very good for small values of ϕ_i at which one would expect the above expression to be accurate. At higher values of ϕ_i, however, the computed mobilities are greater than those predicted from the above theory. One question that immediately arises is whether the observed difference results from an incorrect estimate of the permeability or equivalently $\mathscr{R}$ by (41) and (42) or from the inapplicability of (43) for determining the mobility in partially fixed beds. The diamonds in figure 12 show the values of $(4\pi\mu\mathscr{R})^{-1}$ obtained from numerical simulations of flow through fixed disks by Sangani & Mo (1994). We note that the effective-medium approximation gives quite accurate estimates of $\mathscr{R}$, at least up to $\phi_m = 0.3$, and hence the observed difference between the computed mobility and the effective-medium estimate suggests that (43) fails at higher ϕ_i.

The observation that the computed m_s is greater than $(4\pi\mu h\mathscr{R})^{-1}$ at higher ϕ_i can be explained in terms of lubrication forces. Specifically, the calculation of $\mathscr{R}$ at higher ϕ_i is dominated by lubrication forces arising from the differences in the streamfunction values for neighbouring disks (Sangani & Yao 1988; Sangani & Mo 1994) which makes $\mathscr{R}^{-1} \sim \epsilon^{5/2}$, ϵ being a measure of the average gap width between disks in a concentrated bed. On the other hand, one expects m_s to be dominated by relative motion lubrication which makes $m_s \sim \epsilon^{3/2}$. Note that this contrasts with the case of spherical particles

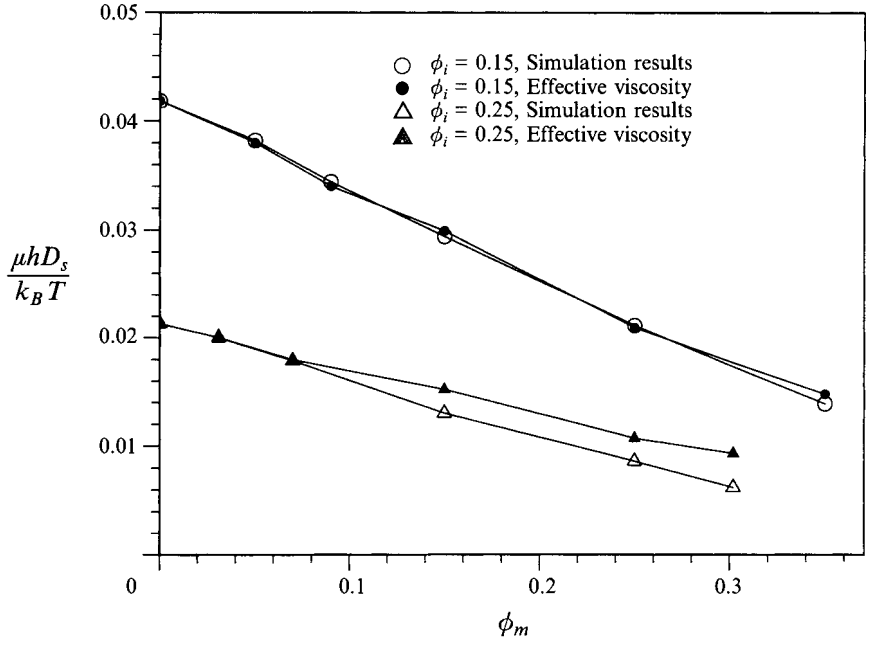

FIGURE 13. The effect of ϕ_m on the short-time diffusivity in partially fixed beds is explained in terms of its effect in modifying the viscosity of the effective medium. The open symbols are the simulation values while the filled symbols are obtained by multiplying the simulation values at $\phi_m = 0$ with the viscosity ratio $\mu/\mu^*(\phi_m)$ given in table 1.

studied by Durlofsky & Brady (1987) for which the lubrication forces are absent from the calculation of $\mathscr{R}$. These investigators also found that while the Brinkman equation gives quite accurate estimates of $\mathscr{R}$ it fails in describing accurately the velocity disturbance caused by a moving spherical particle in a bed of fixed particles at moderate values of ϕ.

The above discussion was restricted to $\phi_m \to 0$. Now we consider the effect of changing ϕ_m on self-diffusivity. As in the case of fully mobile suspensions, we expect this to merely alter the effective viscosity of the suspension. The results from figure 11 are replotted in figure 13 for this purpose and indicated by open circles and triangles. The filled circles and triangles, on the other hand, correspond to an effective-medium approximation in which we take the diffusivity at $\phi_i = 0.15$ and 0.25 with $\phi_m = 0$ from figure 12 and multiply it with μ/μ^* obtained from table 1 for ϕ corresponding to ϕ_m. We see an excellent agreement between computed diffusivities and those estimated from the effective-viscosity data for $\phi_i = 0.15$. At $\phi_i = 0.25$ and higher ϕ_m, however, we observe a consistent overprediction by the effective-medium theory. The screening length predicted by the effective-medium theory in a dense fixed bed is extremely short and consequently it is not too surprising that the effective-medium approximation fails. In addition, we should note that the theory only accounts for the change in viscosity of the suspension due to mobile disks and thus ignores the contribution to the viscosity from fixed disks.

Figure 14 shows the effect of varying ϕ_i keeping the total area fraction ϕ_t constant. We see that diffusivity decreases with increasing ϕ_i. The higher values of ϕ_i reduce the Brinkman screening length and hence the diffusivity.

It is interesting to compare the values of diffusivity in suspensions with a fraction of disks fixed against those in completely mobile suspensions for which the Saffman

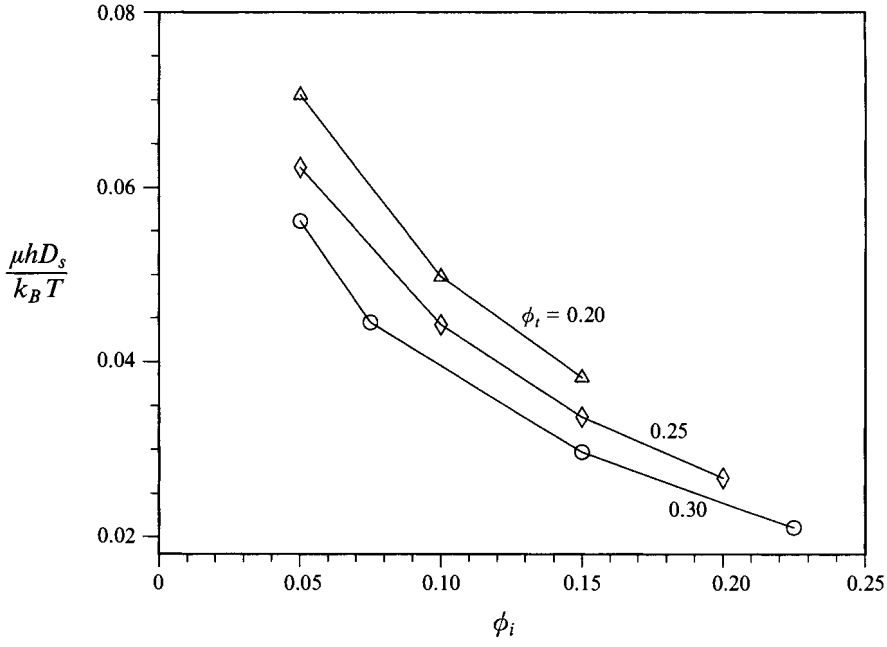

FIGURE 14. Short-time self-diffusivity as a function of ϕ_i at constant ϕ_t.

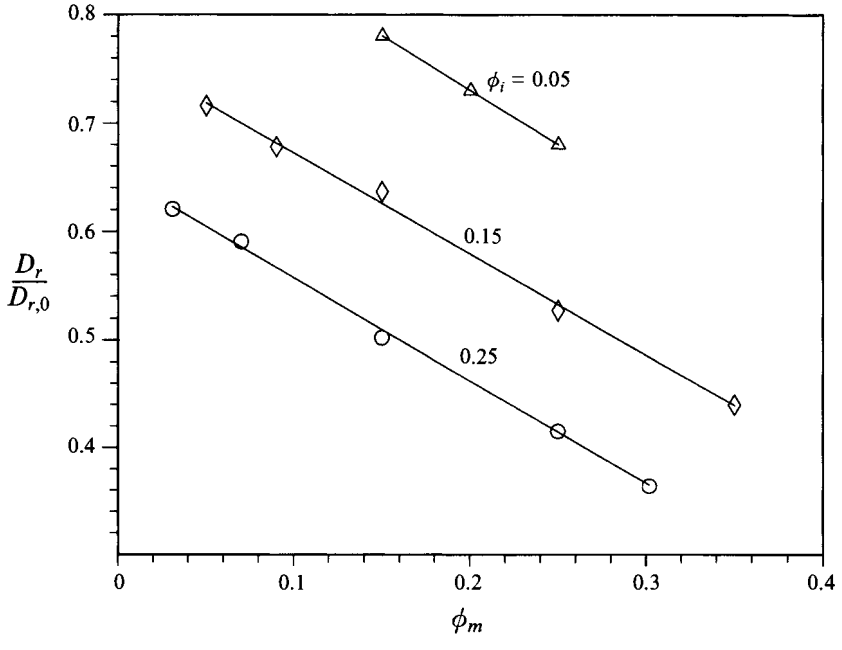

FIGURE 15. Rotational diffusivity as a function of ϕ_m for indicated values of ϕ_i.

screening is important. With $\lambda = 250$ and $\phi_t = 0.05$, a free suspension ($\phi_i = 0$) yields a non-dimensional diffusivity $\mu h D_s / k_B T = 0.365$ while a fixed suspension ($\phi_i = 0.05$) yields 0.094. A further increase of ϕ_i by 0.05 reduces the diffusivity further to 0.054. Similarly, $\phi_m = 0.15$, $\phi_i = 0$ and $\lambda = 250$ gives a non-dimensional diffusivity of 0.308

while $\phi_m = 0.15$ with $\phi_i = 0.05$ yields a diffusivity of 0.071. Thus a larger drop in diffusivity occurs as ϕ_i is increased from zero to 0.05 than from 0.05 to 0.10. Of course in comparing these different values of diffusivity we must keep in mind the relative magnitude of the screening lengths based on Brinkman and Saffman screening. For small ϕ_i, k/a^2 diverges as $-\log(4\phi_i))/(4\phi_i)$. The Brinkman screening length $k^{1/2}$ even at ϕ_i as small as 5×10^{-4} is only $50a$ compared with the typical Saffman screening length of $250a$. In most plasma membranes the fraction of immobilized proteins is about 30% of the total proteins and thus Brinkman screening plays the dominant role.

4.2. *Rotational diffusivity*

Bussell *et al.* (1995*b*) also gave an approximate expression for the rotational diffusivity of a single disk in a partially fixed bed. Their calculation involved solving the Brinkman flow around a rotating disk to yield

$$\frac{D_r}{D_{r,0}} = \left[1+\frac{\alpha K_0(\alpha)}{2K_1(\alpha)}\right]^{-1} = 1-2\phi_i, \tag{44}$$

where $\alpha^2 = a^2/k$. The last equality results from the use of the effective-medium approximation (41) and (42) for the permeability. This calculation was based on equating the Brinkman viscosity to the lipid viscosity and consequently the ratio of rotational diffusivity is independent of ϕ_m.

Figure 15 shows the rotational diffusivity as a function of ϕ_m for three different values of ϕ_i. We see that the diffusivity varies linearly with ϕ_m. These data are therefore fitted according to

$$D_r/D_{r,0} = c_7(\phi_i)+c_8(\phi_i)\,\phi_m \tag{45}$$

and c_7 and c_8 are listed in table 3. We now estimate $D_r/D_{r,0}$ at $\phi_m = 0$ to equal $c_7(\phi_i)$ and compare with the effective-medium approximation (44). At $\phi_i = 0.05$, the low-ϕ_i asymptote (44) predicts the diffusivity ratio to be 0.90 while simulations (c_7 in table 3) give 0.93. Thus we see that assuming the validity of the Brinkman approximation for the whole region outside the disk yields lower diffusivities.

For the translational diffusivity, we found that the reduction in D_s with increasing ϕ_m could be explained in terms of an effective viscosity. We attempt to achieve the same result for the rotational diffusivity in figure 16. Thus we compare the computed values of $D_r/D_{r,0}$ (i.e. $c_7(\phi_i)+\phi_m c_8(\phi_i)$) to the values $c_7(\phi_i)\mu/\mu^*(\phi_m)$ obtained by assuming that the only effect of non-zero ϕ_m is to modify the effective-medium viscosity. The viscosity ratio μ^*/μ is taken from the fourth column in table 1. We see that, unlike the case of translational diffusion, the rotational diffusivities obtained using the effective viscosity are considerably lower than the simulation values.

Both of the above results indicate that the approximations in which the effective Brinkman medium is assumed to apply for the complete region outside the test disk give poor estimates of the rotational diffusivity. This is in contrast to what we found for the translational diffusivity. In the latter case, the interactions are long range in nature since the velocity induced by a translating disk does not decay until Brinkman screening becomes effective. The interactions in the rotational diffusivity problem, on the other hand, are not as long ranged and the discrete nature of the suspension is consequently important.

Figure 17 shows the rotational diffusivity as a function of ϕ_i for constant ϕ_t. This figure also includes $D_r/D_{r,0}$ values for $\phi_i = 0$ taken from the free-suspension simulations. We see a rather smooth transition from the free suspension to the partially fixed suspensions. The decrease in D_r is less severe since the rotational interactions are

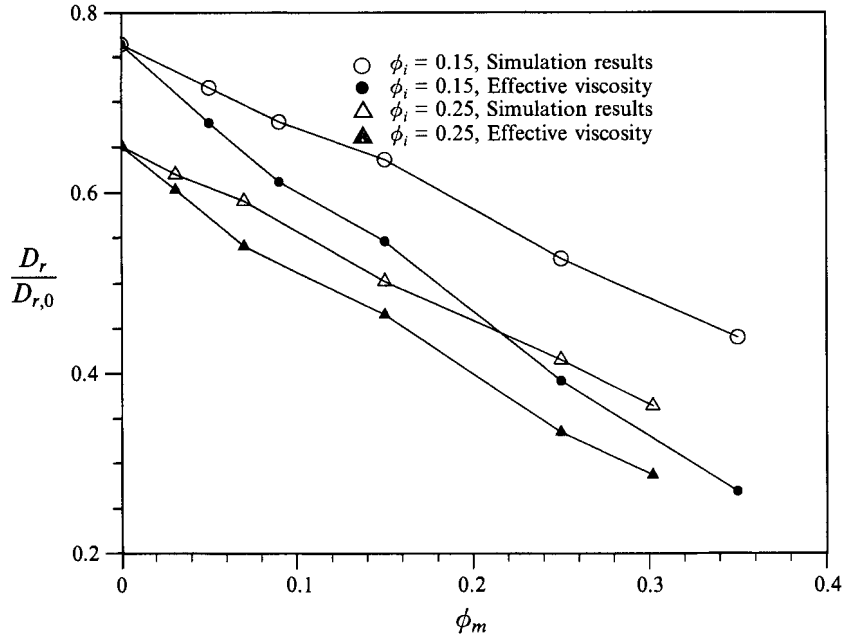

FIGURE 16. The rotational-diffusion analogue of figure 13. The effect of varying ϕ_m cannot be explained in terms of its influence on the effective viscosity of the medium.

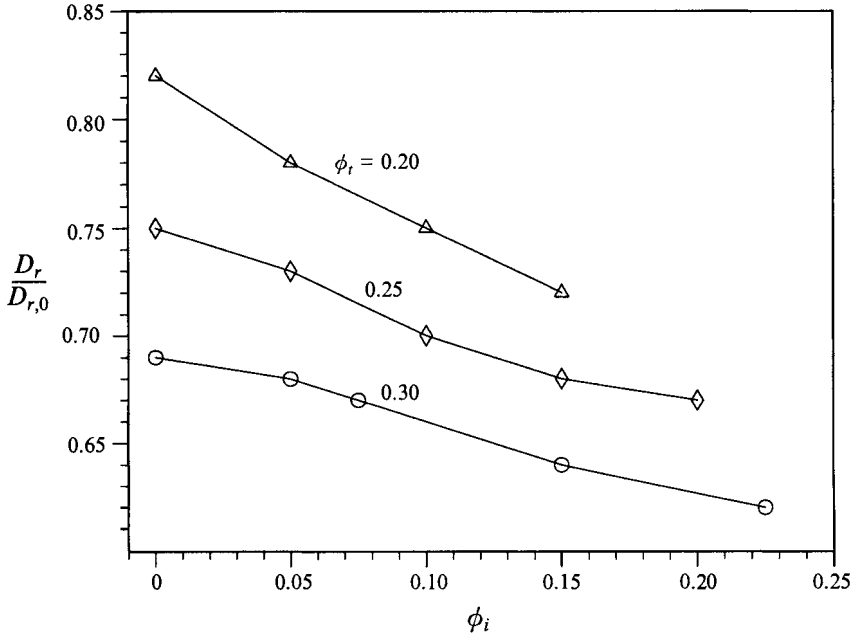

FIGURE 17. Effect of ϕ_i on rotational diffusivity.

short range in both the free and the partially fixed suspensions. This is unlike the case of translational diffusivity which shows a large drop in diffusivity as the screening length changes from λa to $k^{1/2}$.

4.3. *Comparison with experiments*

As in the case of reconstituted membranes, we need to estimate the long-time self-diffusivity in order to compare our simulation results with experiments, We shall assume the validity of (37) and determine the thermodynamic hinderance factor f from simulations of Saxton (1990) which ignore hydrodynamic interactions but account for area exclusion effects and the partial immobilization of the suspension. Since the total area fraction in biological membranes is typically in the range 0.2–0.3, we quote below his results for this range of ϕ_t:

$$\phi_t = 0.30: \quad f = 1.67\phi_m, \tag{46}$$

$$\phi_t = 0.25: \quad f = \begin{cases} 0.08 + 2.6\phi_m & \text{for} \quad \phi_m \leqslant 0.07, \\ 0.15 + 1.6\phi_m & \text{for} \quad 0.07 < \phi_m \leqslant 0.25, \end{cases}$$

$$\phi_t = 0.20: \quad f = \begin{cases} 0.22 + 3.0\phi_m & \text{for} \quad \phi_m \leqslant 0.06, \\ 0.31 + 1.5\phi_m & \text{for} \quad 0.06 < \phi_m \leqslant 0.20. \end{cases}$$

Before presenting a quantitative comparison of the theory with experiments in which the area fraction of immobile protein was varied, it is interesting to note the qualitative difference between diffusion in membranes in the presence and in the absence of cytoskeletal constraints. The membranes of erythrocytes (red blood cells) provide the most direct comparison. The diffusivity of band 3, the most common integral membrane protein, in most types of erythrocytes is about 4.5×10^{-11} cm^2 s^{-1}. However, the diffusivity of band 3 protein in spherocytes, a particular type of erythrocyte in which the cytoskeleton has a minimal effect on the membrane, is 2.5×10^{-9} cm^2 s^{-1} (Sheetz, Schindler & Koppel 1980). Thus, the interaction of the membrane protein with cytoskeleton brings about a 56-fold reduction in the diffusivity. The total area fraction of proteins in these membrane is about 0.17; with 40 % of the proteins immobile in case of most erythrocytes (i.e. $\phi_i \approx 0.07$) and none in spherocytes, our fixed-bed model predicts that an 8-fold decrease in diffusivity will result from the interaction of mobile proteins with the immobile proteins. (This calculation is based on the assumption that the area fraction of band 3 in spherocytes is also 0.17 and that $\lambda = 1000$.) The additional 7-fold decrease in diffusivity observed experimentally may result from the hinderance of the diffusion of mobile proteins resulting from the interaction of the portion of these proteins that protrude into the aqueous phase with the cytoskeleton. In most cells, the total area fraction of proteins is close to 0.3 and the effect of hydrodynamic interactions with immobile proteins will be even more pronounced than in erythrocytes.

Figure 18 shows a comparison with the data of Henis & Elson (1981*a*) for the long-time self-diffusivity of surface immunoglobulins (sIg), a cell surface protein, labelled with monovalent fragments of rabbit anti-mouse IgG in the plasma membrane of mouse lymphocytes. These investigators varied ϕ_i by treating cells with various amounts of concanavalin A which binds receptors containing lectin domains. We assume that the immobilization of sIg, which was reported by these investigators, is representative of the immobilization of all receptors on this cell. Thus, the comparison is based on the assumption of $\phi_t = 0.25$. The lipid viscosity was chosen by requiring that the theory matches one experimental point. We chose the point corresponding to

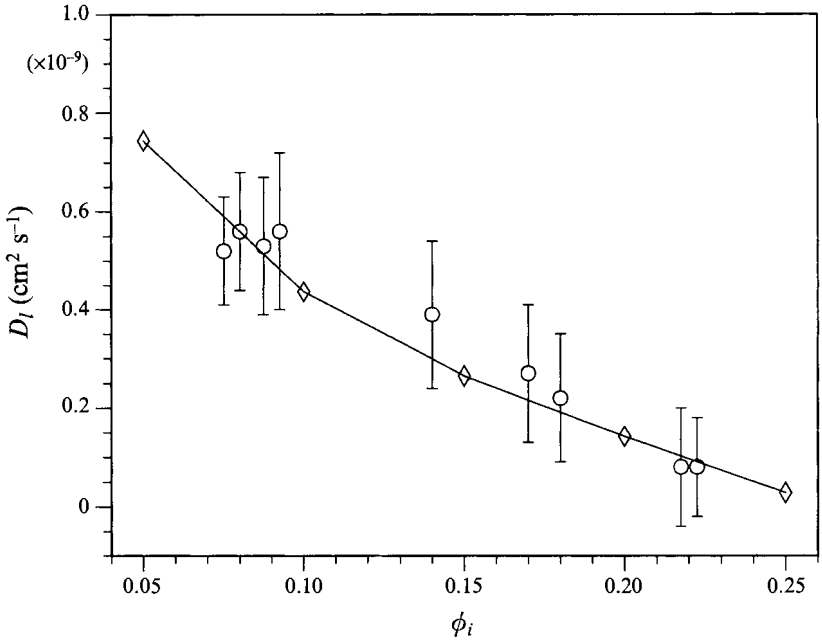

FIGURE 18. Comparison of theory and experiments for the long-time diffusivity of surface immunoglobulins in plasma membranes of mouse lymphocytes. The lipid viscosity was chosen such that the theory and experiments agree at $\phi_i = 0.08$. The theoretical values are indicated by diamonds while the experimental data by Henis & Elson (1981*a*) are indicated by open circles.

$\phi_i = 0.08$, the second lowest area fraction in the figure, because the diffusivity increased slightly (although perhaps within experimental uncertainty) between the first two points. A change in the estimate of μ will shift the curve up or down roughly in proportion to μ. We note that the agreement between the theory and experiments is very good.

Finally, it should be noted that we have presented here a model in which the diffusion of freely mobile proteins in a plasma membrane is retarded solely by hydrodynamic interactions with other, entirely immobilized, proteins. This fixed-bed model predicts a much lower diffusivities found in cell membranes compared with reconstituted membranes. It also compares well with the variation in diffusivity with immobile area fraction observed in Henis & Elson (1981*a*) as the above comparison showed. However, it is likely that other factors (including the interaction of portions of proteins that protrude into the aqueous phase with the cytoskeleton) influence diffusivities in cell membranes. For example, experimental data on cell types other than lymphocytes by Henis & Elson (1981*b*) fail to show the correlation between immobile protein area fraction and protein diffusivity predicted by the model.

5. Conclusions

We have developed a method for numerically simulating hydrodynamic interactions among integral membrane proteins. This is used to determine the short-time self-translational and rotational diffusivities and the gradient diffusivity in both reconstituted and plasma membranes. The results of computations are compared to theoretical predictions of Bussell *et al.* (1994, 1995*a*, *b*) for dilute membranes, and to appropriate effective-medium approximations for non-dilute membranes. An attempt

has also been made to provide some reasons for the observed success or failure of the effective-medium approximation in predicting correct short-time diffusivities. We found that the approximations are adequate for problems in which the interactions are long range, i.e. in predicting self- and collective translational mobility in free suspensions and in partially fixed suspensions at moderate ϕ_i where the Brinkman screening length is large compared to the radius of the disks.

The computed short-time diffusivities adjusted for the thermodynamic effects in an approximate manner using the results of Monte Carlo simulations gave estimated long-time self-diffusivities which were in very good agreement with experimental data on various protein–membrane systems. This represents a significant improvement over previous theories which did not account for the effect of the hydrodynamic interactions of proteins. The comparison required making reasonable estimates of various parameters such as the lipid phase viscosity and the total area fraction. Most of these parameters were estimated from sources independent of the data with which the comparison was made except in some cases where an experimental point was used to fix a system parameter. This was justified since our primary objective was to assess the effect of protein concentration on the diffusivity. However, of course, it would be desirable to have experimental measurements in which independent means of predicting or experimentally determining all the parameters required for comparison with the theory were available.

We should perhaps add here that the experimental data we have chosen for comparison with the theory represents only a small fraction of the data available in the literature, which also include some data on rotational (see e.g. Zidovetzski *et al.* 1986; Myers, Holowka & Baird 1992; Rahman *et al.* 1992) and gradient (McCloskey, Liu & Poo 1984; Young, McCloskey & Poo 1984; Zagyansky & Jard 1979) diffusivities. The experimental uncertainty in many of these data is such that a quantitative comparison with our theory for these diffusivities is not meaningful. From the standpoint of future theoretical developments, it would be desirable to predict the lipid-phase viscosity and to assess the accuracy of the approximation (37) which decoupled the effects of hydrodynamic and thermodynamic interactions on long-time diffusivity. We hope to address the latter in future work by carrying out Stokesian simulations and determining the trajectory of each protein through Langevin equation as outlined by Ermak & McCammon (1978) and Brady & Bossis (1988).

This work was supported by the National Science Foundation grants BCS-8958632 to D.A.H., CTS-8857565 to D.L.K., and CTS-9118675 and CTS-9307723 to A.S.S. The computations were performed on the Cornell National Supercomputer Facility.

Appendix

To determine the lubrication force multipoles, we carry out a detailed analysis of the flow in the narrow gap between two disks. Because of the linearity of the governing equations, this can be done by solving each of the problems listed in figure 19 separately. Denoting the upper and lower disks by γ and α respectively, and $\Delta U_n = (\boldsymbol{U}^\gamma - \boldsymbol{U}^\alpha)\cdot\boldsymbol{n}$, $\Delta U_t = (\boldsymbol{U}^\gamma - \boldsymbol{U}^\alpha)\cdot\boldsymbol{t}$, $\Omega_m = \frac{1}{2}(\Omega^\gamma + \Omega^\alpha)$, and $\Delta\Omega = \frac{1}{2}(\Omega^\gamma - \Omega^\alpha)$, where $\boldsymbol{n}$ is the unit vector along $\boldsymbol{x}^\gamma - \boldsymbol{x}^\alpha$, and $\boldsymbol{t}$ is the unit tangent vector normal to $\boldsymbol{n}$, we write

$$\psi = \epsilon^{1/2}\Delta U_n \psi_A + \epsilon(\Delta U_t \psi_B + \Omega_m \psi_C + \Delta\Omega\psi_D), \tag{A 1}$$

where $\psi_A - \psi_D$ are determined by solving the problems A–D shown in figure 19. Scaling

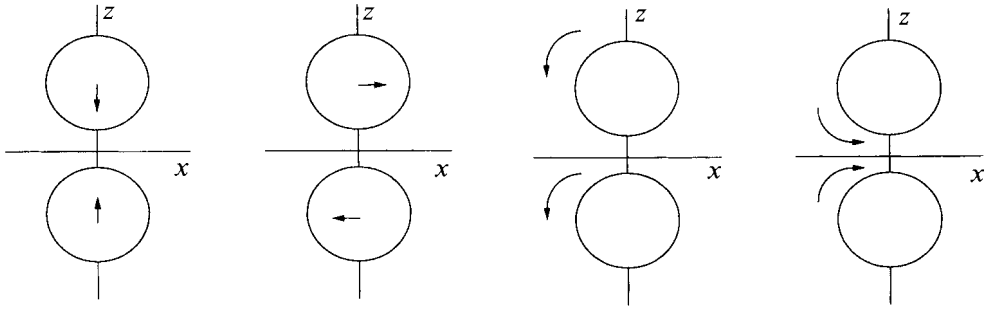

FIGURE 19. The lubrication problems A–D.

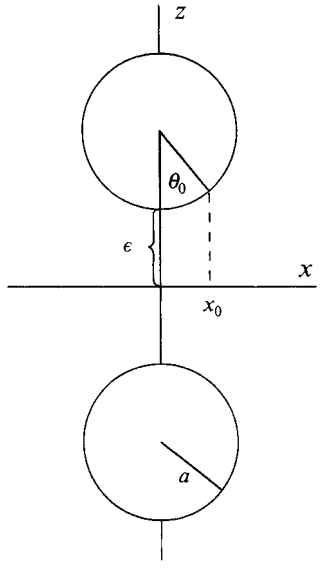

FIGURE 20. A schematic of the local coordinate system for analysing various lubrication problems.

the distances in the tangent and normal direction by $\epsilon^{1/2}$ and ϵ, respectively (figure 20), and carrying out standard lubrication analyses yields

$$\psi_A = x\left[\frac{z^3}{4h^3}-\frac{3z}{4h}+\epsilon\left\{z^5\left(\frac{3}{5h^5}-\frac{3}{8h^4}\right)-z^3\left(\frac{3}{8h^4}+\frac{9}{20h^3}-\frac{3}{8h^2}\right)+z\left(\frac{3}{8h^2}-\frac{3}{20h}\right)\right\}+O(\epsilon^2)\right], \tag{A 2}$$

$$\psi_B = \frac{z^2}{4h}+\frac{h-1}{4}+\epsilon\left\{z^4\left(\frac{1}{6h^3}-\frac{1}{8h^2}\right)+z^2\left(\frac{1}{8}-\frac{1}{12h}-\frac{1}{8h^2}\right)-\frac{h-1}{12}\right\}+O(\epsilon^2), \tag{A 3}$$

$$\psi_C = \frac{z^2}{2h}+\epsilon\left\{z^4\left(\frac{1}{3h^3}-\frac{1}{4h^2}\right)+z^2\left(\frac{1}{3h}-\frac{1}{4}-\frac{1}{4h^2}\right)\right\}+O(\epsilon^2), \tag{A 4}$$

$$\psi_D = z^3\left(\frac{1}{2h^2}-\frac{2}{3h^3}\right)+z\left(-\frac{1}{2}+\frac{2}{h}\right)+\epsilon\left\{z^5\left(-\frac{1}{2h^3}+\frac{2}{h^4}-\frac{8}{h^5}\right)\right.$$
$$\left.+z^3\left(-\frac{4}{3h^2}+\frac{7}{6h^3}+\frac{1}{4h^4}-\frac{1}{12h}\right)+z\left(\frac{h}{4}-\frac{1}{h}-\frac{1}{h^2}\right)\right\}+O(\epsilon^2), \tag{A 5}$$

where $h = 1+\frac{1}{2}x^2$. Note that the surface of the particles in this scaled coordinate system is given by

$$z = \pm Z(x) = \pm[h+\tfrac{1}{2}\epsilon(h-1)^2+O(\epsilon^2)]. \tag{A 6}$$

Now the momentum equation can be integrated after substituting for the velocity components in terms of the streamfunction to obtain expressions for pressure and the force density distribution at the surface of the particles. For example, writing $\boldsymbol{f}^{lub} = f_x^{lub}\boldsymbol{t}+f_z^{lub}\boldsymbol{n}$, with

$$f_x^{lub,\alpha} = \mu[\Delta U_n f_x^A+\Delta U_t f_x^B+\Omega_m f_x^C+\Delta\Omega f_x^D], \tag{A 7}$$

and a similar expression for $f_z^{lub,\alpha}$, we obtain

$$f_x^A = \frac{x}{\epsilon^{3/2}}\left[-\frac{3}{4h^2}+\epsilon\left\{\frac{3}{4h}-\frac{33}{20h^2}+\frac{3}{4h^3}\right\}+O(\epsilon^2)\right], \tag{A 8}$$

$$f_z^A = \frac{1}{\epsilon^2}\left[\frac{3}{4h^2}+\epsilon\left\{\frac{12}{5h^2}-\frac{3}{4h^3}\right\}+O(\epsilon^2)\right], \tag{A 9}$$

$$f_x^B = \frac{1}{\epsilon}\left[\frac{1}{h}+\epsilon\left\{\frac{1}{2}+\frac{2}{3h}-\frac{1}{2h^2}\right\}+O(\epsilon^2)\right], \quad f_z^B = O(\epsilon), \tag{A 10}$$

$$f_x^C = \frac{1}{\epsilon}\left[\frac{1}{h}+\epsilon\left\{\frac{3}{5h}-\frac{1}{2h^2}\right\}+O(\epsilon^2)\right], \quad f_z^C = O(\epsilon), \tag{A 11}$$

$$f_x^D = \frac{1}{\epsilon}\left[-\frac{1}{h}+\frac{2}{h^2}+\epsilon\left\{-\frac{1}{2}-\frac{8}{h}+\frac{9}{h^2}-\frac{4}{h^3}\right\}+O(\epsilon^2)\right], \tag{A 12}$$

$$f_z^D = \frac{x}{\epsilon^{3/2}}\left[\frac{1}{h^2}+\epsilon\left\{\frac{2}{h^2}-\frac{3}{2h}-\frac{1}{h^3}\right\}+O(\epsilon^2)\right]. \tag{A 13}$$

The lubrication force density on disk γ can be obtained by combining the above expressions with the symmetry properties for each of the problems.

In computations we take the lubrication force density to be non-zero and given by the above expressions only for $-x_0 \leqslant x \leqslant x_0$ on each disk with $\theta_0 = \epsilon^{1/2}x_0$ a suitably chosen small number. The lubrication force, stresslet, and torque on each disk are evaluated by integrating the above force density over this range of x_0, e.g.

$$\boldsymbol{F}^{lub,\alpha} = \epsilon^{1/2}\int_{-x_0}^{x_0} \boldsymbol{f}^{lub,\alpha}[1+\epsilon(h-1)]\,\mathrm{d}x. \tag{A 14}$$

For example, the lubrication force on disk α due to relative motion along $\boldsymbol{n}$ is given by $\mu\Delta U_n F^A$, where

$$F^A = \frac{1}{\epsilon^{3/2}}\left[\frac{3}{4}J+\frac{3x_0}{4h_0}+\epsilon\left\{\frac{207}{80}J+\frac{87}{80}\frac{x_0}{h_0}-\frac{3x_0}{8h_0^2}\right\}+O(\epsilon^2)\right], \tag{A 15}$$

with $h_0 = 1+\frac{1}{2}x_0^2$ and

$$J = \sqrt{2}\tan^{-1}(x_0/\sqrt{2}). \tag{A 16}$$

For fixed θ_0 and $\epsilon \to 0$, (A 15) yields $F^A \to 3\pi[1+69\epsilon/20+O(\epsilon^2)]/(2(2\epsilon)^{3/2})$. This is in agreement with the result presented by Bussell *et al.* (1992). (Note that ϵ in the results presented by these authors equals the gap width and not the half-gap width as suggested by their figure 7.)

The lubrication force multipoles $\boldsymbol{A}_{(n)}$ can be determined now by substituting for the lubrication force density in (10). The problems A–C give non-zero lubrication

multipoles only for even n while the problem D gives a contribution to odd-ordered multipoles. In the present study we evaluate $A_{(n)}$ up to $n = 3$. Substituting for force density in (10) and using symmetry properties for various problems yields, for example,

$$\boldsymbol{A}_{(2)} = \boldsymbol{nt}B_{nt} + \boldsymbol{nn}\,B_{nn}, \tag{A 17}$$

where

$$B_{nt} = \frac{\epsilon^{3/2}\Delta U_n}{\pi\mu}\int_0^{x_0}[Zf_z^A + \epsilon^{-1/2}xf_x^A][1+\epsilon(h-1)]\,\mathrm{d}x, \tag{A 18}$$

$$B_{nn} = \frac{\epsilon^{3/2}}{\pi\mu}\int_0^{x_0} Z[\Delta U_t f_x^B + \Omega_m f_x^C][1+\epsilon(h-1)]\,\mathrm{d}x. \tag{A 19}$$

In deriving the above expression for B_{nt}, we have made use of the fact that only the symmetric part of $\boldsymbol{A}_{(2)}$ is relevant since ψ^{lub} depends only on the scalar product of the tensor with $\nabla\nabla S_2$. Upon substituting for f_x^A and f_z^A into (A 18) and carrying out the integration, we obtain

$$B_{nt} = \frac{\Delta U_n x_0}{\pi\epsilon^{1/2}}\left[\frac{3}{4h_0} + \epsilon\left\{-\frac{3}{4} + \frac{27J}{16x_0} - \frac{3}{80h_0} - \frac{3}{4h_0^2}\right\}\right], \tag{A 20}$$

where $h_0 = 1+\frac{1}{2}x_0^2$. As $\epsilon \to 0$ keeping $\theta_0 = \epsilon^{1/2}x_0$ fixed, $B_{nt} \to \Delta U_n/\pi[3/(2\theta_0) - 3\theta_0/4]$. Thus, even though the leading-order lubrication force due to the relative velocity along $\boldsymbol{n}$ is $O(\epsilon^{-3/2})$, the deviatoric lubrication force dipole is only $O(1)$. The two leading-order contributions of $O(\epsilon^{-1/2})$ from f_z^A and f_x^A cancel resulting in a smaller, $O(1)$, contribution to the lubrication force dipole.

Expressions for B_{nn} and the other lubrication force multipoles are obtained in a similar manner.

As mentioned in the main text, we choose x_0 as a function of ϵ such that the computed results agree with the known results for a pair of particles for which exact calculations are available from Bussell *et al.* (1992). In computations, we chose different values of x_0 for each of the lubrication multipoles. These values were chosen such that our results for pair of particles match the results of Bussell *et al.* After fixing x_0, we carried out calculations for random arrays with $N_p = 9$ for which exact results could be obtained by using $N_s = 15$. It was found that the computed results with $N_s = 4$ and lubrication multipoles to $n = 3$ were accurate to better than 5%.

REFERENCES

Abney, J. R., Scalettar, B. A. & Owicki, J. C. 1989 Self diffusion of interacting membrane proteins. *Biophys. J.* **55**, 817–833.

Axelrod, D., Koppel, D. E., Schlessinger, J., Elson, E. & Webb, W. W. 1976 Mobility measurements by analysis of fluorescence photobleaching recovery kinetics. *Biophys. J.* **16**, 1055–1069.

Batchelor, G. K. 1976 Brownian diffusion of particles with hydrodynamic interactions. *J. Fluid Mech.* **74**, 1–29.

Batchelor, G. K. 1982 Sedimentation in a dilute polydisperse system of interacting spheres. Part 1. General theory. *J. Fluid Mech.* **119**, 379–408.

Brady, J. F. 1984 The Einstein viscosity correction in n dimensions. *Intl J. Multiphase Flow* **10**, 113–114.

Brady, J. F. 1994 The long-time self-diffusivity in concentrated colloidal dispersions. *J. Fluid Mech.* **272**, 109–134.

Brady, J. F. & Bossis, G. 1988 Stokesian dynamics. *Ann. Rev. Fluid Mech.* **20**, 111–157.

Brady, J. F. & Durlofsky, L. J. 1988 The sedimentation rate of disordered suspensions. *Phys. Fluids* **31**, 717–727.

BRINKMAN, H. C. 1947 A calculation of the viscous force exerted by a flowing fluid on a dense swarm of particles. *Appl. Sci. Res.* A 1, 27–34.

BUSSELL, S. J., KOCH, D. L. & HAMMER, D. A. 1992 The resistivity and mobility functions for a model system of two equal-sized proteins in a lipid bilayer. *J. Fluid Mech.* **243**, 679–697.

BUSSELL, S. J., KOCH, D. L. & HAMMER, D. A. 1994 The effect of hydrodynamic interactions on the tracer and gradient diffusion of integral membrane proteins in lipid bilayers. *J. Fluid Mech.* **258**, 167–190.

BUSSELL, S. J., KOCH, D. L. & HAMMER, D. A. 1995*a* The effect of hydrodynamic interactions on the diffusion of integral membrane proteins: tracer diffusion in organelle and reconstituted membranes. *Biophys. J.* (in press).

BUSSELL, S. J., KOCH, D. L. & HAMMER, D. A. 1995*b* The effect of hydrodynamic interactions on the diffusion of integral membrane proteins: diffusion in plasma membranes. *Biophys. J.* (in press).

CHAE, D. G., REE, F. H. & REE, T. 1969 Radial distribution functions and equation of state of the hard-disk fluid. *J. Chem. Phys.* **50**, 1581–1589.

CHAZOTTE, B. & HACKENBROCK, C. R. 1988 The multicollisional, obstructed, long-range diffusional nature of mitochondrial electron transport. *J. Bio. Chem.* **263**, 14359–14367.

DEATHERAGE, J. F., HENDERSON, R. & CAPALDI, R. A. 1982 Relationship between membrane and cytoplasmic domains in cytochrome c oxidase by electron microscopy in media of different density. *J. Mol. Biol.* **158**, 501–514.

DURLOFSKY, L. & BRADY, J. F. 1987 Analysis of the Brinkman equation as a model for flow in porous media. *Phys. Fluids* **30**, 3329–3341.

EINSTEIN, A. 1906 A new determination of molecular dimensions. *Ann. Physik* **19**, 289–306 (and Corrections **34**, 591–592 (1911)).

ERMAK, D. L. & MCCAMMON, J. A. 1978 Brownian dynamics with hydrodynamic interactions. *J. Chem. Phys.* **69**, 1352.

HASIMOTO, H. 1959 On the periodic fundamental solution of the Stokes equations and their application to viscous flow past a cubic array of spheres. *J. Fluid Mech.* **5**, 317–328.

HENDERSON, R. & UNWIN, P. N. T. 1975 Three-dimensional model of purple membrane obtained by electron microscopy. *Nature* **257**, 28–32.

HENIS, Y. I. & ELSON, E. L. 1981*a* Inhibition of the mobility of mouse lymphocyte surface immunoglobins by locally bound concanavalin A. *Proc. Natl Acad. Sci. USA* **78**, 1072–1076.

HENIS, Y. I. & ELSON, E. L. 1981*b* Differences in the response of several cell types to inhibition of surface receptor mobility by local concanavalin A binding. *Exp. Cell Res.* **136**, 189–201.

HINCH, E. J. 1977 An averaged-equation approach to particle interactions in a fluid suspension. *J. Fluid Mech.* **83**, 695–720.

HOWELLS, I. D. 1974 Drag due to the motion of a Newtonian fluid through a sparse random array of small fixed objects. *J. Fluid Mech.* **64**, 449–475.

KOPS-WERKHOVEN, M. M. & FIJNAUT, H. M. 1981 Dynamic light scattering and sedimentation experiments on silica dispersions at finite concentrations. *J. Chem. Phys.* **74**, 1618.

KOPS-WERKHOVEN, M. M., VRIJ, A. & LEKKERKERKER, H. N. W. 1983 On the relation between diffusion, sedimentation, and friction. *J. Chem. Phys.* **78**, 2760.

LADD, A. J. C. 1988 Hydrodynamic interactions in suspensions of spherical particles. *J. Chem. Phys.* **88**, 5051.

LADD, A. J. C. 1989 Hydrodynamic interactions and the viscosity of suspensions of freely moving spheres. *J. Chem. Phys.* **90**, 1149.

LADD, A. J. C. 1990 Hydrodynamic transport coefficients of random dispersions of hard spheres. *J. Chem. Phys.* **93**, 3484–3493.

LEONARD, K., HAIKER, H. & WEISS, H. 1987 Three-dimensional structure of NADH: ubiquinone reductase (complex I) from Neoropora mitochondria determined by electron microscopy of membrane crystals. *J. Mol. Biol.* **194**, 277–286.

MCCLOSKEY, M. A., LIU, Z-Y. & POO, M.-Y. 1984 Lateral electromigration and diffusion of Fce receptors on rat basophilic leukemia cells: effect of IgG binding. *J. Cell Biol.* **99**, 778–787.

MEDINA-NOYALA, M. 1988 Long-time self-diffusion in concentrated colloidal dispersions. *Phys. Rev. Lett.* **60**, 2705–2708.

METZGAR, H. & KINET, J. P. 1988 How antibodies work; focus on F_c receptors. *Fed. Am. Soc. Exp. Biol. J.* **2**, 3–11.

MO, G. & SANGANI, A. S. 1994 A method of computing Stokes flow interactions among spherical objects and its application to suspensions of drops and porous particles. *Phys. Fluids* **6**, 1637–1652.

MYERS, J. N., HOLOWKA, D. & BAIRD, B. 1992 Rotational motion of monomeric and dimeric immunoglobulin E-receptor complexes. *Biochemist* **31**, 567–575.

PETERS, R. & CHERRY, R. J. 1982 Lateral and rotational diffusion of bacteriorhodopsin in lipid bilayers: experimental test of the Saffman-Delbruck equations. *Proc. Natn Acad. Sci. USA* **79**, 4317–4321.

PHILLIPS, R. J., BRADY, J. F. & BOSSIS, G. 1988 Hydrodynamic transport properties of hardsphere dispersions. I. Suspensions of freely mobile particles. *Phys. Fluids* **31**, 3462–3472.

RAHMAN, N. A., PECHT, I., ROESS, D. A. & BARISAS, B. G. 1992 Rotational dynamics of type I Fce receptors on individually-selected rat mast cells studied by polarized fluorescence depletion. *Biophys. J.* **61**, 334–346.

RALLISON, J. M. 1988 Brownian diffusion in concentrated suspensions of intracting particles. *J. Fluid Mech.* **186**, 471–500.

SAFFMAN, P. G. 1976 Brownian motion in thin sheets of viscous fluid. *J. Fluid Mech.* **73**, 593–602.

SAFFMAN, P. G. & DELBRÜCK, M. 1975 Brownian motion in biological membranes. *Proc. Natn Acad. Sci. USA* **72**, 3111–3113.

SANGANI, A. S. & MO, G. 1994 Inclusion of lubrication forces in dynamic simulations. *Phys. Fluids* **6**, 1653–1662.

SANGANI, A. S. & YAO, C. 1988 Transport processes in random arrays of cylinders. II. Viscous flow. *Phys. Fluids* **31**, 2435–2444.

SAXTON, M. J. 1987 Lateral diffusion in an archipelago: the effect of mobile obstacles. *Biophys. J.* **52**, 989–997.

SAXTON, M. J. 1990 Lateral diffusion in a mixture of mobile and immobile particles: a monte carlo study. *Biophys. J.* **58**, 1303–1306.

SCALLETAR, B. A. & ABNEY, J. R. 1991 Molecular crowding and protein diffusion in biological membranes. *Comments Mol. Biophys.* **7**, 79–107.

SHEETZ, M. P., SCHINDLER, M. & KOPPEL, D. E. 1980 Lateral mobility of integral membrane proteins in increased spherocytic erythrocytes. *Nature* **285**, 510–512.

YOUNG, S. H., MCCLOSKEY, M. & POO, M.-M. 1984 Migration of cell surface receptors induced by extracellular electric fields: Theory and applications. *The Receptors* **1**, 511–539.

ZAGYANSKY, Y. A. & JARD, S. 1979 Does lectin-receptor complex formation produce zones of restricted mobility within the membranes? *Nature* **280**, 591.

ZIDOVETZSKI, R., BARTHOLDI, M., ARNDT-JOVIN, D. & JOVIN, T. M. 1986 Rotational dynamics of F_c receptor for immunoglobulin E on histamin-releasing rat basophilic leukemia cells. *Biochemist* **25**, 4397–4401.